DOI 10.1515/revic-2012-0003 — Rev Inorg Chem 2012; 32(2-4): 81–100

Yao Chen and Shengqian Ma*

Microporous lanthanide metal-organic frameworks

Abstract: Microporous metal-organic frameworks (MOFs) based on lanthanide metal ions or clusters represent a group of porous materials, featuring interesting coordination, electronic, and optical properties. These attractive properties in combination with the porosity make microporous lanthanide MOFs (Ln-MOFs) hold the promise for various applications. This review is to provide an overview of the current status of the research in microporous Ln-MOFs, and highlight their potential as types of multifunctional materials for applications in gas/solvent adsorption and separation, luminescence and chemical sensing and catalysis.

Keywords: catalysis; gas adsorption; lanthanide MOF; luminescence; microporous; sensor.

***Corresponding author: Shengqian Ma**, Department of Chemistry, University of South Florida, 4202 E. Fowler Avenue, Tampa, FL 33620, USA, e-mail: sqma@usf.edu
Yao Chen: Department of Chemistry, University of South Florida, 4202 E. Fowler Avenue, Tampa, FL 33620, USA

Introduction

Microporous lanthanide metal-organic frameworks (Ln-MOFs) continue to attract an escalating attention in the MOF research area, owing to their unique optical, magnetic properties and characteristic coordination preferences of lanthanide metal ions and related clusters. Compared with first-row transition metal ions, they usually exhibit high coordination number and connectivity, which could facilitate the formation of stable three-dimensional networks. The lanthanide-based luminescence has been of intense interest over decades. However, the luminescence studies of Ln-MOFs have largely been conducted until recently. Compared with the discrete molecular lanthanide complexes, Ln-MOFs are attractive because of their high thermal stability and high luminescence output. Luminescence can be enhanced by both the lanthanide metal centers and the organic linker. The quantum yield, intensity and brightness can also be increased by the antenna effect, which could be induced by the interaction between the metal and ligand (Moore et al. 2009, Rocha et al. 2011). In addition, the microporosity of Ln-MOFs offers the opportunity for fine-tuning of the luminescence behavior by trapping molecules in the framework to influence the lanthanide emission, and the relative high surface areas of microporous Ln-MOFs also suggest it could serve both as a preconcentrator and detection medium. Therefore, chemical sensing represents a promising application of Ln-MOFs. Microporous Ln-MOFs are also promising candidates for heterogeneous catalysis application, since lanthanide ions have a flexible coordination sphere and can create coordinatively unsaturated metal centers, and the high surface areas of them represent another advantage benefiting their catalytic performances. Additionally, the permanent microporosity, together with tunable pore sizes of Ln-MOFs, affords them potential for applications in gas/solvent storage or separation. Indeed, over the past decade, a remarkable amount of effort has been dedicated to developing microporous Ln-MOFs as types of multifunctional materials for various applications (Table 1) (Reineke et al. 1999, Snejko et al. 2002, Wang et al. 2002, 2008, 2011, Deluzet et al. 2003, Ghosh and Bharadwaj 2004, Zhao et al. 2004, Chen et al. 2005, Guo et al. 2005, 2006a, Gándara et al. 2007, Rieter et al. 2007, Huang et al. 2009, Kostakis et al. 2009, Liao et al. 2009, Lim et al. 2009, Rocha et al. 2009, White et al. 2009b, Zhao et al. 2009a,b,c,d, Han et al. 2010, Jiang et al. 2010a, Khan et al. 2010, Lan et al. 2010, Lee et al. 2010, Lin et al. 2010, Pereira et al. 2010, Silva et al. 2010, Cai et al. 2011, Datcu et al. 2011, Gu et al. 2011, Liu et al. 2011, Nayak et al. 2011, Sun et al. 2011, Yang et al. 2011a, Knope et al. 2012).

The aim of this review is to give a broad overview of recent developments of functional microporous Ln-MOFs, with focus on their interesting properties and potential applications, such as gas/solvent adsorption and separation, luminescence and chemical sensing, and catalysis.

Lanthanide	Ligand	Properties and potential applications	References
Dy, Er, Y, Yb	TATB	Microporosity, thermal stability, gas adsorption	Ma et al. 2008, Ma et al. 2009
Er, Tm	BDC	Microporosity, gas adsorption, luminescence sensing	Reineke et al. 1999, Guo et al. 2006b, Rieter et al. 2007, Han et al. 2010, He et al. 2010, Xu et al. 2011
Nd, Sm, Eu, Gd, Tb, Ho, Er, Dy, Yb	BTC	Microporosity, thermal stability, luminescence properties, gas/solvent adsorption, luminescent sensing, catalysis	Rosi et al. 2005, Guo et al. 2006a, 2010, Luo et al. 2008, Gustafsson et al. 2010, Jiang et al. 2010b, Khan et al. 2010
Er, Eu, Tb, Ce	NDC	Luminescence properties	Wang et al. 2002, Deluzet et al. 2003
La, Pr, Nd	1, 5-NDS/2, 6-NDS	Thermal stability, optical properties, catalysis	Snejko et al. 2002, Gándara et al. 2007
Yb and Er	H_2pvdc	Luminescent properties (sensitization of NIR)	Lim et al. 2009, White et al. 2009a
Y, La, Pr, Nd, Sm, Eu, Gd, Tb,Dy, Ho, Er	H_2cmp	Photoluminescence and catalysismagnetic properties	Cunha-Silva et al. 2009, Pereira et al. 2010
Yb, Eu, Gd, Tb, Dy, Ho and Er	BPT	Microporosity, magnetism, luminescence, NIR	Guo et al. 2011
Tb	BTB	Microporosity	Devic et al. 2005
Y, La, Ce, Pr, Nd, Sm, Eu, Gd, Tb, Dy, Ho, Er, Yb	H_2hfipbb	Luminescence and heterogeneous catalysis	Gándara et al. 2008
Eu	H_2hfipbb	Microporosities, magnetic properties, sensor	Harbuzaru et al. 2008
Pr, Eu, Gd, Tb, Dy	N-H_2BDC	Photoluminescent and magnetic properties	Black et al. 2009
Y, Ce, Sm, Eu, Tb, Gd, Er;	H_5hedp	Photoluminescence	Rocha et al. 2009
Ce, Tb, Dy	H_2pydc	Microporosity, magnetic properties	Chen et al. 2008a, Silva et al. 2010
Sm, Eu, Gd, Yb, Nd, Er	ntb	Microporosity, thermal stability, selective adsorption	Jiang et al. 2010b, Lan et al. 2010
La, Ce, Nd	pdc	Fluorescence properties	Ghosh and Bharadwaj 2004, Wang et al. 2008
Ce, Nd, Sm, Eu, Tb, Dy	pda	Microporosity, luminescence, catalytic activity, magnetic properties	Zhao et al. 2004, Zhao et al. 2009a,b, Ren et al. 2011
Nd, Sm, Eu, Gd, Tb, Dy, Ho, Er, Yb, Pr	TDC	Luminescence and magnetic properties	Huang et al. 2009, Sun et al. 2011, Wang et al. 2011
Eu, Gd	TTP	Luminescence and anion exchange	Yang et al. 2011b
Pr, Nd	H_2ATPT	Microporosity, gas/solvent adsorption	Chen et al. 2005
Nd, Eu	phen	Microporosity	Liao et al. 2009
Eu	H_2phenDCA	Microporosity, pH sensing	Harbuzaru et al. 2009
La, Ce, Pr, Nd, Gd	dhbdc	Magnetic properties	Nayak et al. 2011
Ce, Nd	m-$BDTH_2$	Magnetic properties	Kostakis et al. 2009
Yb, Tb, Dy, Ho, Er, Tm	CTC	Microporosity, fluorescence, adsorption, magnetic properties	Zhao et al. 2009a,b
Nd, Sm, Eu, Gd	H_3TPO	Microporosity, gas adsorption	Lee et al. 2010
Gd, Tb, Dy	IDC	Microporosity, tunable luminescent properties	Lu et al. 2009
Gd, Dy	TDA	Ferromagnetic coupling and slow magnetic relaxation behavior	Chen et al. 2009a
Yb	AQDS	Catalysis	Gándara et al. 2009
Tb, Ho, Er, Y	bpdc	Luminescence	Guo et al. 2005
La, Sm, Eu, Gd, Dy, Ho, Er, Yb	H_3ImDC	Photoluminescent properties	Gu et al. 2011
Sm, Tb, Er, Yb	H_3PPA	Luminescent sensing	Knope et al. 2012
Eu, Tb	H_2pzdc	Luminescence, microporosity	Cai et al. 2011
Yb, Tb	OBA	Luminescent sensing	Lin et al. 2010

(*Table 1 continued*)

Lanthanide	Ligand	Properties and potential applications	References
Sm, Eu, Gd	Hcbmp	Luminescent properties	Liu et al. 2011
Dy, Ho, Er	hpzc	Magnetic properties	Chen et al. 2008b
Sm, Eu, Gd, Tb, Dy	PTMTC	Luminescence and magnetism	Roques et al. 2008, Datcu et al. 2011

Table 1 Properties and potential applications for selected lanthanide metal-organic frameworks (MOFs).
TATB, 4,4′,4″-s-triazine-2,4,6-triyl-tribenzoate; BDC, 1,4-benzenedicarboxylate; BTC, 1,3,5-benzenetricarboxylate NDC, 2,6-naphthalenedicarboxylate; 1,5-NDS, 1,5-naphthalenedisulfonate; 2,6-NDS, 2,6-naphthalenedisulfonate; H_2pvdc, 4,4-[(2,5-dimethoxy-1,4-phenylene)-di-2,1-ethenediyl]bisbenzoic acid; H_2cmp, (carboxymethyl)iminodi(methylphosphonic acid); BPT, biphenyl-3,4′,5-tricarboxylate; BTB, 1,3,5-benzenetrisbenzoate; H_2hfipbb, 4,4′-(hexafluoroisopropylidene)bis(benzoic acid); N-H_2BDC, 2-amino-1,4-benzenedicarboxylic acid; H_5hedp, etidronic acid; H_2pydc, 2,5-pyridinedicarboxylic acid; ntb, tris-(benzimidazol-2-ylmethyl) amine; pdc, pyridine-2,6-dicarboxylate; pda, 1,4-phenylenediacetate; TDC, thiophene- 2,5-dicarboxylate; TTP, 1,1′,1″-(2,4,6-trimethylbenzene-1,3,5-triyl)tris(methylene)tripyridinium-4-olate; H_2ATPT, 2-aminoterephthalic acid; phen, 1,1′-phenanthroline; H_2phenDCA, 1,1′-phenanthroline-2,9-dicarboxylic acid; dhbdc, benzene-2,5-dihydroxy-1,4-dicarboxylate; m-$BDTH_2$, 1,3-benzeneditetrazol-5-yl; CTC, cis, cis-1,3,5-cyclohexanetricarboxylic acid; H_3TPO, tris-(4-carboxylphenyl)phosphineoxide; IDC, imidazole-4,5-dicarboxylate; TDA, thiophene-2,5-dicarboxylic acid anion; AQDS, anthraquinone-2,6-disulfonate; bpdc, 4,4′-biphenyldicarboxylic acid; H_3ImDC, 4,5-imidazoledicarboxylic acid; H_3PPA, phosphonoacetic acid; H_2pzdc, pyrazinedicarboxylic acid; OBA, 4,4′-oxybis(benzoate); Hcbmp, 2-(carboxylic acid)-6-(2-benzimidazolyl) pyridine; hpzc, 3-hydroxypyrazine-2-carboxylate; PTMTC, polychlorotriphenylmethyl tricarboxylate radical.

Gas/solvent adsorption of microporous Ln-MOFs

Porous MOFs possess some merits which are beneficial for gas/solvent sorption application, such as high surface areas (Férey 2008), uniform and tunable pore sizes. In addition, a variety of chemical compositions and topologies allow the optimization of adsorption properties via rational design and syntheses of targeted MOFs (Ma et al. 2010). To this point, microporous Ln-MOFs have recently been explored for applications in gas/solvent adsorption.

Among different types of organic ligands employed for the construction of Ln-MOFs, carboxylate-based linkers are of particular interest due to their high propensity to afford porous structures. Utilizing some polytopic carboxylates, Rosi et al. designed and synthesized a series of Ln-MOFs with rod packing motifs. Among those structures, Tb-1,3,5-benzenetricarboxylate (Tb-BTC, MOF-76) demonstrated permanent microporosity and molecular sieving behaviors, as revealed from the sorption isotherms of different gas/solvent molecules (N_2, Ar, CH_2Cl_2, C_6H_6, C_6H_{12}). The rod shaped secondary building units (SBUs) play a role of efficiently preventing the interpenetration, thus enabling accessible porosity of MOF-76 (Rosi et al. 2005). Also, using BTC ligand, Luo et al. prepared a porous rare-earth MOF, Y-BTC [$Y(BTC)(H_2O)\cdot 4.3H_2O$], under solvothermal conditions (Luo et al. 2008). This Y-MOF possesses tetragonal pores with a size of approximately 6 Å, and it exhibited highly selective sorption behavior of dihydrogen over dinitrogen. The pore size of ~6 Å has been suggested to maximize the interactions between the H_2 molecules and the pore walls, thus leading to a high volumetric hydrogen uptake capacity of 28.8 g/L at 77 K and 10 bar. Because of the similarity of lanthanide metal ions, a series of isostructural microporous Ln-MOFs enantiomers, $Ln(BTC)(H_2O)\cdot[\text{dimethylformamide DMF})]_{1.1}$ (Ln=Y, Tb Dy, Er and Yb) with interesting (6,6)-connected topology were reported by Jiang et al. (2010a). These Ln-MOF structures feature free windows of 6~7 Å with accessible exposed metal sites, and exhibited moderate surface areas but high thermal stability (over 450°C) (Figure 1). Another interesting example of BTC-based Ln-MOF is $Dy(BTC)(H_2O)\cdot DMF$, reported by Guo et al. (2006a). The dissociation of the guest and terminal coordinated molecules in the Dy-BTC MOF rendered the permanent porosity and accessible Lewis acid sites, which afforded interesting performances in hydrogen adsorption, sensing, and catalysis. Extending the BTC ligand to the 1,3,5-benzenetrisbenzoate (BTB) ligand, Devic et al. (2005) reported a 3D microporous Ln-MOF, MIL 103 [$Tb(BTB)(H_2O)\cdot 2(C_6H_{12}O)$] and the guest-free MIL-103 exhibited a typical type I isotherm, with a Langmuir surface area over 1000 m^2g^{-1} and pore size larger than 10 Å (Figure 2).

The porosity of MOFs plays an important role in their properties (such as gas/solvent adsorption, catalysis, sensing or drug delivery), and the extension of ligand length has been widely used to increase the porosity, but sometimes may lead to interpenetration of the frameworks. The control of interpenetration using different strategies

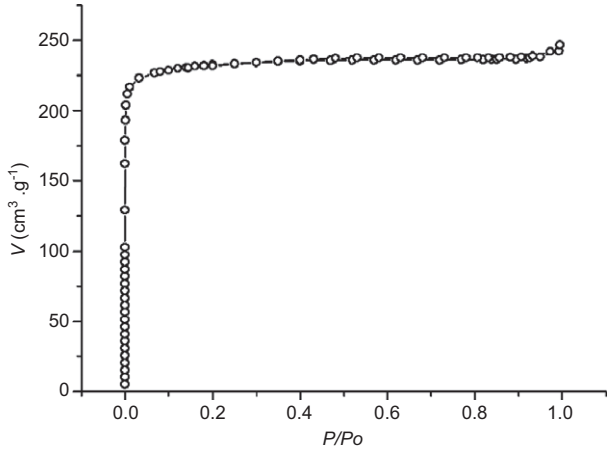

Figure 1 Nitrogen gas adsorption isotherm at 77 K for MIL-103 degassed overnight at 150°C. P/P_0 is the ratio of gas pressure (P) to saturation pressure (P_0=750 mm Hg). V is the adsorbed volume. [Reprinted with permission from Jiang et al. (2010), Copyright © 2010 American Chemical Society.]

has been reported, and recently also extended to Ln-MOFs (Kondo et al. 2000, Rosi et al. 2005, Ma et al. 2007, Ma and Lin 2008, Shekhah et al. 2009, Zhang et al. 2009, Farha et al. 2010). He et al. reported the first example of the control of interpenetration in Ln-MOFs (He et al. 2010). They constructed a series of porous noninterpenetrated Ln-MOFs [$Er_2(BDC)_3(phen)_2{\cdot}3H_2O$, $Tm_2(TBDC)_3(DMF)_2(H_2O)_2{\cdot}4H_2O$ and $Er_2(TBDC)_3(phen)_2{\cdot}4DMF{\cdot}2H_2O$], by using a sterically bulky ligand and a terminal chelating ligand to replace BDC and coordinated solvent molecules (Scheme 1). The sterically

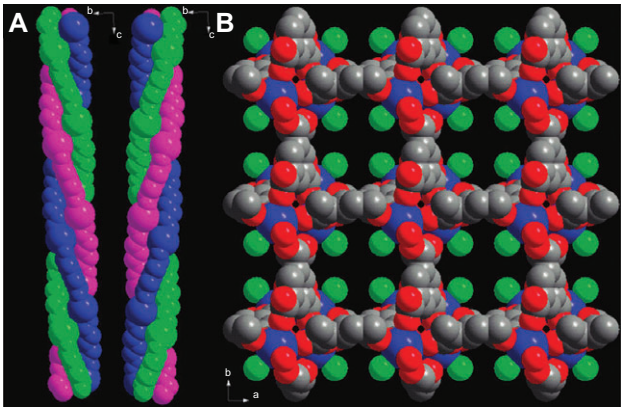

Figure 2 (A) Left-handed and right-handed helical chains along the c-axis in enantiomers. (B) View of the 3D structure with P4322 space group along the c-axis, exhibiting 1D helical channels of about 6–7 Å for each side, and accessible Ln^{3+} sites can be obtained after removing the coordinated aqua molecules, which are denoted as green. The H atoms and free dimethylformamide (DMF) molecules are omitted for clarity; Ln, O, and C atoms are drawn as blue, red, and gray circles, respectively. [Reprinted with permission from Devic et al. (2005), Copyright © 2005 American Chemical Society.]

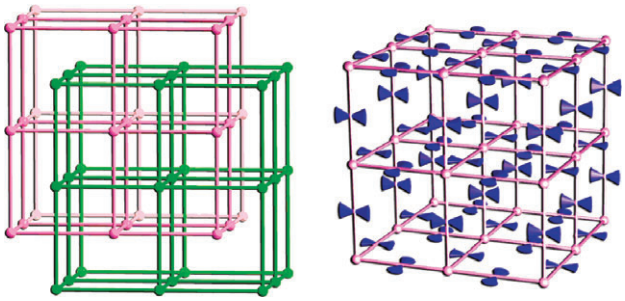

Scheme 1 Schematic representation of the interpenetrating net (left) and the noninterpenetrating net constructed with an organic ligand with a large steric-hindrance group (right). [Reprinted with permission from He et al. (2010), Copyright © 2010 American Chemical Society.]

bulky groups from the ligands not only prevented the interpenetration of the frameworks, but also facilitated the generation of microporous Ln-MOFs with wavy channels and a limited aperture for passage of guest molecules, which lead to selective gas sorption properties via the molecular sieving effect.

Although interpenetration could reduce the porosity, it may increase the wall thickness and constrict the pore size of the framework, thus resulting in enhancement of thermal stability. This has been exemplified by a doubly interpenetrated microporous framework, PCN-17, which was synthesized and characterized by Zhou and co-workers for selective gas adsorption applications (Ma et al. 2008). The lanthanide ytterbium ion was used to coordinate with H_3TATB (TATB=4,4′,4″-S-triazine-2,4,6-triyl tribenzoate) ligand to form PCN-17 ($Yb_4(\mu_4\text{-}H_2O)(C_{24}H_{12}N_3O_6)_{8/3}(SO_4)_2{\cdot}3H_2O{\cdot}10DMSO$) in DMSO at 145°C for 72 h. The sulfate bridging ligand was used to coordinatively link the doubly interpenetrated frameworks and further reduce the pore size (Figure 3). Therefore, the framework possesses ultramicropores with pore sizes around 3.5 Å (excluding van der Waals radii) and demonstrated high thermal stability of up to ~480°C, which could be attributed to the coordinatively linked interpenetration in the microporous 3D framework (Scheme 2). In addition, PCN-17 exhibited uncommon selective adsorption of O_2 over N_2, H_2 over CO, and H_2 over N_2 (Figure 4), which originates from the molecular sieving effect exerted by the small pore size (~3.5 Å). The same group also extended this system to other lanthanide metal ions, and constructed a series of isostructural microporous Ln-MOFs: PCN-17(Dy), PCN-17(Er), PCN-17(Y), and PCN-17(Yb) with similar coordinatively linked interpenetration (Ma et al. 2009). The shrinking of their unit cell parameters followed the lanthanide contraction trend. TGA profiles indicated that these Ln-MOFs possess high thermal

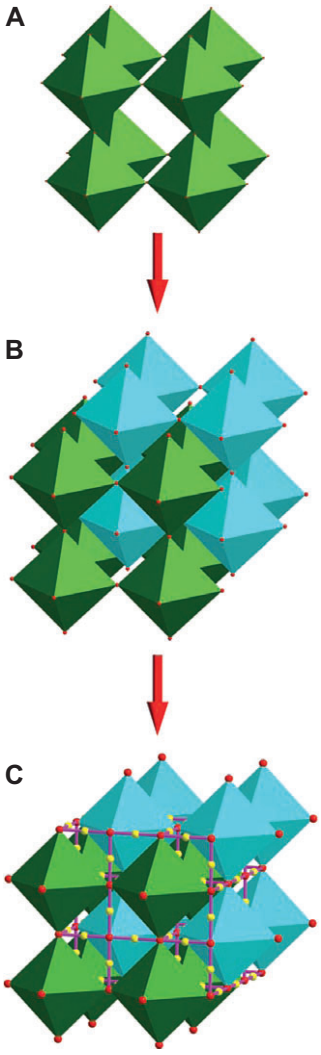

Figure 3 (A) A single (8,3)-net. (B) Doubly interpenetrated nets. (C) Through sulfate bridges coordinatively linked interpenetrated framework (yellow spheres represent sulfur and red spheres represent the square-planar SBU). [Reprinted with permission from Ma et al. (2008), Copyright © 2008, Wiley-VCH.]

stability (up to 550°C), and that all of these Ln-MOFs possess confined pore sizes, which afford interesting selective gas adsorption properties.

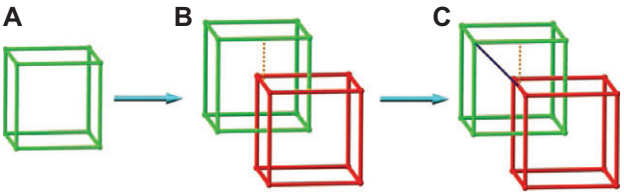

Scheme 2 (A) A single net. (B) Two doubly interpenetrated nets. (C) Interpenetrated nets linked by a coordinative bond. The vertical gold dotted line represents a π-π interaction; the blue solid line represents coordinative bonding. [Reprinted with permission from Ma et al. (2008), Copyright © 2008, Wiley-VCH.]

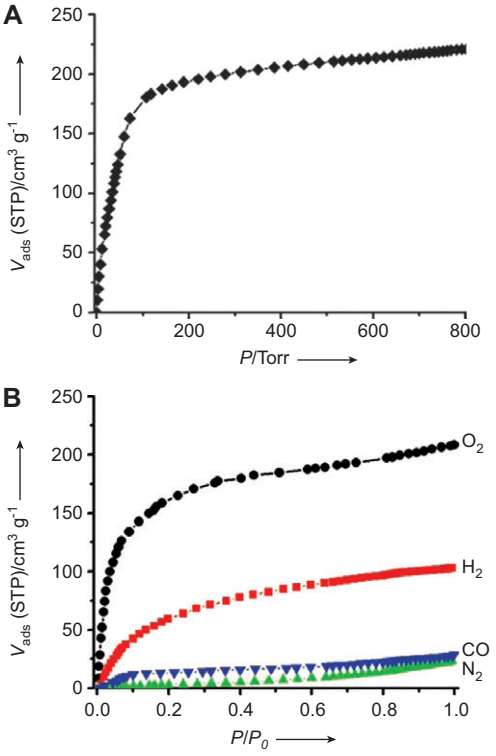

Figure 4 Gas-adsorption isotherms of the activated PCN-17. (A) CO_2 at 195 K; (B) H_2, O_2, N_2, and CO at 77 K (for H_2, P_0 represents a relative standard; STP: standard temperature and pressure..). [Reprinted with permission from Ma et al. (2008), Copyright © 2008, Wiley-VCH.]

Owing to different intermolecular forces in the precursor solution, such as ionic interactions, hydrogen bonding, and π-π interactions, MOFs can easily aggregate to form amorphous particles or condensed solids without porosity during the reaction processes. The utilization of a structure-directing agent such as a template for the arrangement of different components into long-range ordered frameworks, or for the construction of the porous structures, represents a way to control the structure and porosity of MOFs (de Lill et al. 2005, Ni et al. 2006, Taylor et al. 2008a,b, deKrafft et al. 2009, Liang et al. 2009, McHale et al. 2010, Tanaka et al. 2010). However, this strategy faces the challenge of maintaining the integrity and the porosity of the structure after removal of the template molecules which are encapsulated in the crystal lattice. Recently, a template-free, coordination-directed assembly method was proposed by Zhang et al. for synthesis and stabilization of porous Ln-MOFs (Ln=Eu, Gd, Yb) (Zhang et al. 2011). The Ln-MOFs were synthesized using a series of different π-conjugated dicarboxylate ligands with different alkyl side-chains (L1-L8) (Scheme 3). The functionalization of ligands by long alkyl side chains has been proven to be an effective strategy to prevent the aggregation of

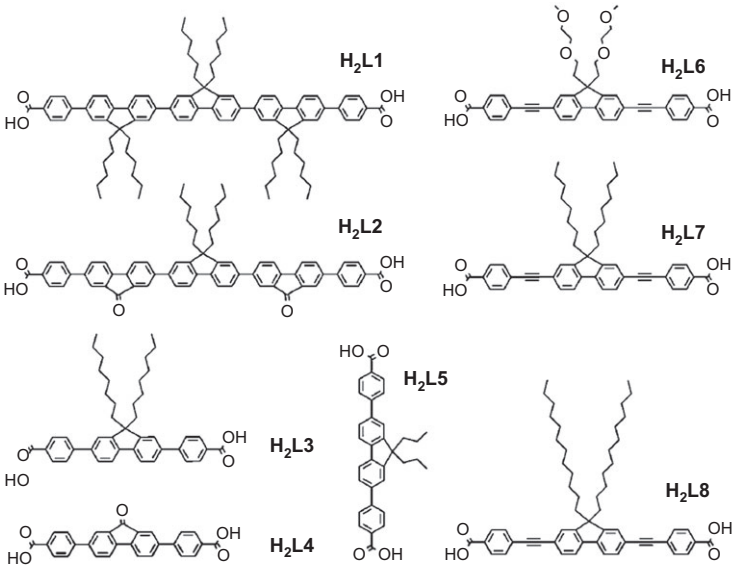

Scheme 3 Chemical structures of the ligands with different π-conjugation lengths and side chains. [Reprinted with permission from Zhang et al. (2011), Copyright © 2011, Wiley-VCH.]

the Ln-MOF nanoparticles and lead to a more crystalline structure (Figure 5). Those Ln-MOFs indicated excellent porosity with large windows, which endow them potential for various applications.

Besides porosity, the enhancement of the heats of adsorption is another critical component in improving gas adsorption performances (e.g., H_2, CO_2) of Ln-MOFs at ambient temperature. It has been well established

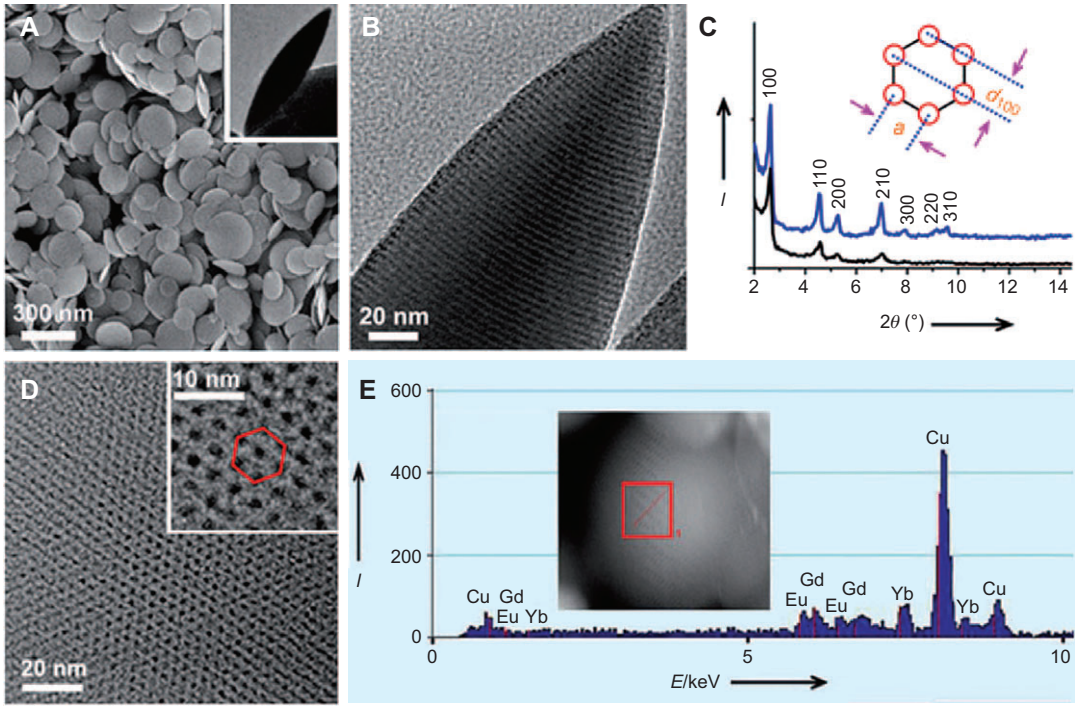

Figure 5 (A) SEM and TEM (inset) images of Eu–L1. (B) HRTEM side view of a representative Eu–L1 particle showing the ordered nanochannels. (C) XRD data of Eu–L1 (black) and Eu–Gd–Yb–L1 (blue) nanoparticles. Inset: schematic illustration showing the relationship between the lattice constant a and d_{100} of the hexagonal packed pattern. (D) HRTEM image of an Eu–Gd–Yb–L1 nanoparticle, inset: magnified view of the hexagonal packed pores. (E) EDAX data measured by STEM mode. The data are collected from the region marked with a red square. [Reprinted with permission from Zhang et al. (2011), Copyright © 2011, Wiley-VCH.]

that coordinatively unsaturated metal sites can provide stronger binding for gas molecules than H-bonding interactions or dispersion forces, and the immobilization of unsaturated metal centers into porous frameworks has been extensively explored to increase the gas uptake capacities of MOFs. Mohapatra et al. (2009) reported the embedding of alkali metal ions into a 3D Ln-MOF {[KHo(C_2O_4)$_2$(H_2O)$_4$]n} (Figure 6), which exhibited permanent porosity with size selective vapor adsorption properties and high storage capabilities for H_2 and CO_2 after the removal of the K-bound water aqua ligands. As a result of the exposure of the unsaturated K-sites on the pore surfaces, the Ln-MOF indicated high heats of adsorption for H_2 (approx. -10 kJ/mol).

Luminescence and sensing

Lanthanide metal ions feature their intricate and characteristic optical properties due to the gradual filling of their 4f orbitals (Table 2) (Binnemans 2009, Eliseeva and Bünzli 2010) from $4f^0$ to $4f^{14}$, which generates a variety of electronic levels (Figure 7). The light-emitting properties of Ln^{3+} make Ln-MOFs hold the promise for the development of light-emitting devices and tunable luminescent sensors.

Luminescence of microporous Ln-MOFs

Although the lanthanide-based luminescence has been intensively exploited over decades, luminescent Ln-MOFs are still at the early stage of development (Cui et al. 2012). There are several features which distinguish microporous Ln-MOFs from other luminescent materials. Owing to the electronic [Xe]$4f^n$ configurations (n = 0–14) of Ln^{3+}, a rich variety of electronic levels can be generated and the energies are well defined due to the shielding of the 4f orbitals by the filled $5s^25p^6$ subshells (Figure 7). Therefore, lanthanide metal ions are less sensitive to the chemical environments in which the lanthanide ions are inserted. As a corollary, each Ln^{3+} exhibits narrow and recognizable 4f-4f transitions. Most lanthanide ions can generate luminescent emissions from ultraviolet (UV) to visible and near-infrared (NIR) ranges (Table 3) (Bünzli et al. 2010). Moreover, lanthanide metal ions exhibit long lifetimes of the excited state, which enables the applications of time-resolved detection or luminescence microscopy (Connally and Piper 2008).

However, due to the forbidden f-f transitions, the direct excitation of lanthanide ions can only provide weak light adsorption, which is a drawback for the applications of lanthanide luminescence. Ln-MOFs offer a variety of

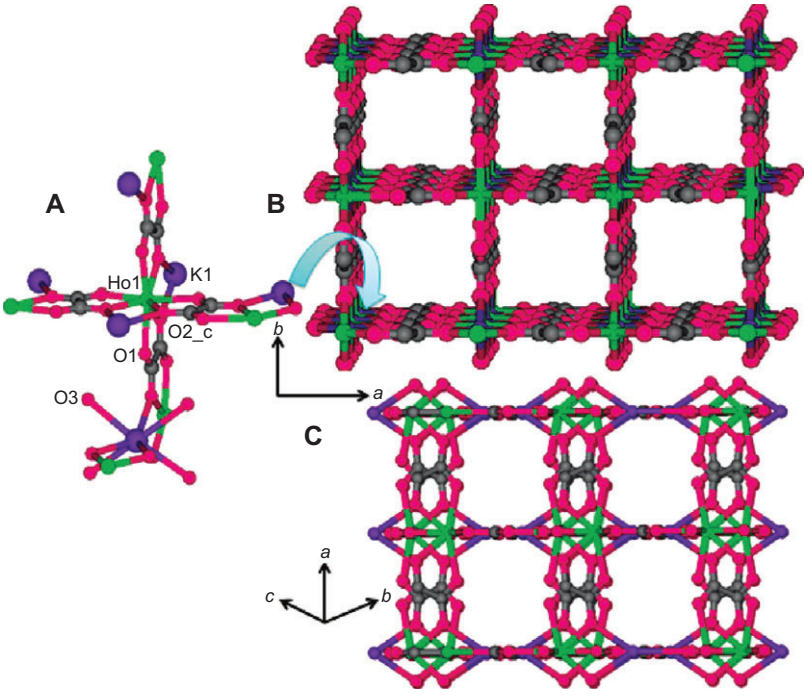

Figure 6 (A) View of the coordination environment of Ho^{III} and K^I in {KHo(C_2O_4)2(H_2O)$_4$}n (1). (B) View of the 3D framework of 1 showing square shaped channel along the crystallographic c axis. (D) View of the 3D framework along parallel to a-axis showing small channels. K-bound water molecules were removed. [Reprinted with permission from Mohapatra et al. (2009), Copyright © 2009 American Chemical Society.]

Element	Symbol	Atomic number (Z)	Configuration Ln^{3+}	Ground state Ln^{3+}
Lanthanum	La	57	[Xe]	$^1S_0$
Cerium	Ce	58	[Xe]$4f^1$	$^2F_{5/2}$
Praseodymium	Pr	59	[Xe]$4f^2$	$^3H_4$
Neodymium	Nd	60	[Xe]$4f^3$	$^4I_{9/2}$
Promethium	Pm	61	[Xe]$4f^4$	$^5I_4$
Samarium	Sm	62	[Xe]$4f^5$	$^6H_{5/2}$
Europium	Eu	63	[Xe]$4f^6$	$^7F_0$
Gadolinium	Gd	64	[Xe]$4f^7$	$^8S_{7/2}$
Terbium	Tb	65	[Xe]$4f^8$	$^7F_6$
Dysprosium	Dy	66	[Xe]$4f^9$	$^6H_{15/2}$
Holmium	Ho	67	[Xe]$4f^{10}$	$^5I_8$
Erbium	Er	68	[Xe]$4f^{11}$	$^4I_{15/2}$
Thulium	Tm	69	[Xe]$4f^{12}$	$^3H_6$
Ytterbium	Yb	70	[Xe]$4f^{13}$	$^2F_{7/2}$
Lutetium	Lu	71	[Xe]$4f^{14}$	$^1S_0$

Table 2 Electronic structure of lanthanide ions. [Reprinted with permission from Binnemans (2009), Copyright © 2009 American Chemical Society.]

strategies for the excitations, because both the lanthanide ions and the organic ligands can provide sources to generate luminescence, and metal-ligand charge transfer related luminescence can contribute to another dimension of luminescence (Scheme 4). Sometimes, guest-induced luminescence can also play an important role in the luminescent functionalities.

The ligand-to-metal charge transfer (LMCT), metal-to-ligand charge transfer (MLCT), and 4f-5d transitions can funnel energy onto the lanthanide ions. Among the diverse forms of energy transfers within MOFs, luminescence sensitization or the antenna effect has been widely explored. Three steps are involved in this process: light absorbance by the organic ligands around the lanthanide ions, energy transfer from organic ligands to the lanthanide ions, and then luminescence generation from the lanthanide ions. It is noteworthy that, because of the stabilization within MOFs, the fluorescence properties (such as fluorescence intensity, lifetimes, and quantum efficiencies) of organic linkers within MOFs frameworks may differ from those of the free molecules after the coupling with Ln^{3+}. In addition, energy transfers from one lanthanide ion to another have also been observed to enhance the luminescence intensity in heterolanthanide MOFs.

Indeed, Ln-MOFs feature predictable structures and tunable luminescence, and the porosity of MOFs could afford multifunctionalities (Chandler et al. 2007). Currently, the luminescent applications of Ln-MOFs focus on targeted chemical sensors, light-emitting devices and biomedical related detections.

One of the important features for microporous Ln-MOFs lies in that the guest molecules in the pores can have a significant influence on their luminescent properties. Wen et al. reported two guest molecule induced luminescent porous Ln-MOFs, $[Ln_2(fumarate)_2(oxalate)(H_2O)_4]\cdot 4H_2O$ (Ln=Eu, Tb) (Zhu et al. 2007) in which reversible changes of luminescence intensities upon de-/rehydration of the frameworks were observed (Figure 8). Water molecules within the frameworks were found to enhance the luminescence significantly and this kind of luminescence upon water adsorption affords potential for

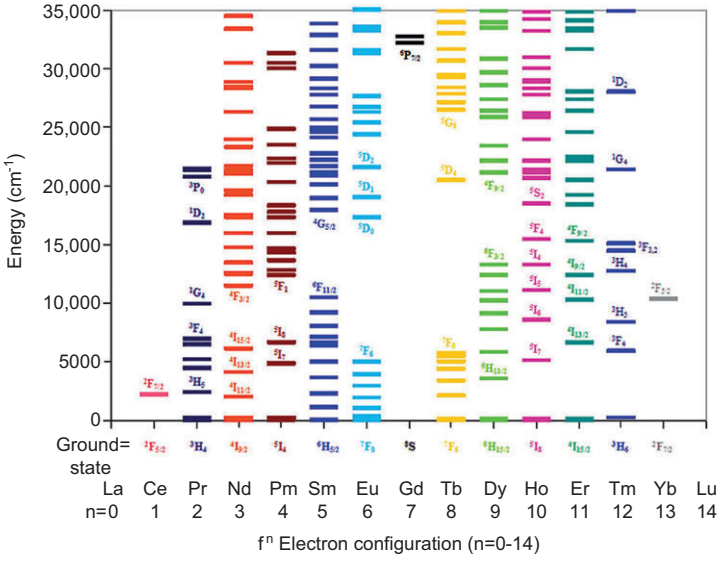

Figure 7 A summary of electronic excited-state energy levels for the Ln(III) series. [Reprinted with permission from Binnemans (2009), Copyright © 2009 American Chemical Society.]

Ln	G[a]	I[a]	F[a]	λ/μm or nm[b]	gap/cm^{-1}[b]	τ^{rad}/ms[b]
Ce	$^2F_{5/2}$	5d	$^2F_{5/2}$	tunable, 300–450		
Pr	$^3H_4$	$^1D_2$	$^3F_4$, $^1G_4$, $^3H_4$, $^3H_5$	1.0, 1.44, 600, 690	6940	(0.05[c]–0.35)
		$^3P_0$	^3H_J (J=4–6)	490, 545, 615	3910	(0.003[c]–0.02)
		$^3P_0$	^3F_J (J=2–4)	640, 700, 725		
Nd	$^4I_{9/2}$	$^4F_{3/2}$	^4I_J (J=9/2–13/2)	900, 1.06, 1.35	5400	0.42 (0.2–0.5)
Sm	$^6H_{5/2}$	$^4G_{5/2}$	^6H_J (J=5/2–13/2)	560, 595, 640, 700, 775	7400	6.26
		$^4G_{5/2}$	^6F_J (J=1/2–9/2)	870, 887, 926, 1.01, 1.15		
		$^4G_{5/2}$	$^6H_{13/2}$	877		
Eu[d]	$^7F_0$	$^5D_0$	^7F_J(J=6–0)	580, 590, 615, 650, 720, 750, 820	12,300	9.7 (1–11)
Gd	$^8S_{7/2}$	$^6P_{7/2}$	$^8S_{7/2}$	315	32,100	10.9
Tb	$^7F_6$	$^5D_4$	^7F_J(J=0–6)	490, 540, 580, 620	14,800	9.0 (1–9)
				650, 660, 675		
Dy	$^6H_{15/2}$	$^4F_{9/2}$	^6H_J(J=15/2–9/2)	475, 570, 660, 750	7850	1.85 (0.15–1.9)
		$^4F_{15/2}$	^6H_J(J=15/2–9/2)	455, 540, 615, 695	1000	3.22[b]
Ho	$^5I_8$	$^5S_2$	^5I_J(J=8,7)	545, 750	3000	0.37 (0.51[c])
		$^5F_5$	$^5I_8$	650	2200	0.8[c]
		$^5F_5$	$^5I_7$	965		
Er[e]	$^4I_{15/2}$	$^4S_{3/2}$	^4I_J(J=15/2, 13/2)	545, 850	3100	0.7[c]
		$^4F_{9/2}$	$^4I_{15/2}$	660	2850	0.6[c]
		$^4I_{9/2}$	$^4I_{15/2}$	810	2150	4.5[c]
		$^4I_{13/2}$	$^4I_{15/2}$	1.54	6500	0.66 (0.7–12)
Tm	$^3H_6$	$^1D_2$	$^3F_4$, $^3H_4$, $^3F_3$, $^3F_2$	450, 650, 740, 775	6650	0.09
		$^1G_4$	$^3H_6$, $^3F_4$, $^3H_5$	470, 650, 770	6250	1.29
		$^3H_4$	$^3H_6$	800	4300	3.6[c]
Yb	$^2F_{7/2}$	$^2F_{5/2}$	$^2F_{7/2}$	980	10,225	2.0 (0.5–2.0)[f]

Table 3 Selected luminescent properties of lanthanide ions. [Reprinted with permission from Bünzli (2010), Copyright © 2010 American Chemical Society.]

[a]G, ground state; I, main emissive state; F, final state; gap, energy difference between I and the highest SO level of F. [b]Values for the equations, (Rosi et al. 2005) [b]otherwise stated, and ranges of observed lifetimes in all media, if available, between parentheses. [c]Doped in Y_2O_2 or in $YLiF_4$(Ho), or in $YAl_3(BO_3)_4$ (Dy). [d]Luminescence from $^5D_1$, $^5D_2$, and $^5D_3$ is also sometimes observed. [e]Luminescence from four other states has also been observed: $^4D_{5/2}$, $^2P_{3/2}$, $^4G_{11/2}$, $_2H_{9/2}$. [f]Complexes with organic ligends: 0.5–1.3 ms; (Luo et al. 2008, Jiang et al. 2010); solid-state inorganic compound: ≈2 ms.

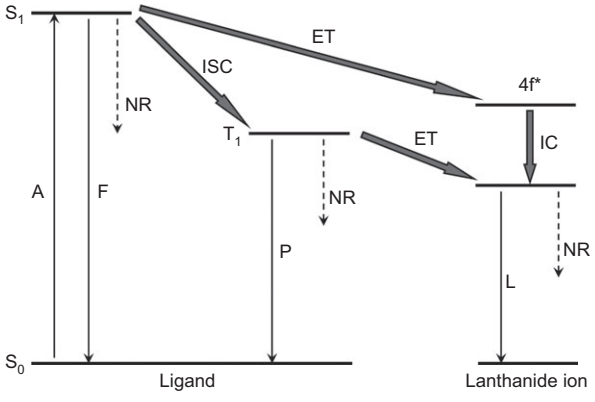

Scheme 4 Schematic representation of energy absorption, migration, emission, and processes in MOFs. A, absorption; F, fluorescence; P, phosphorescence; L, lanthanide-centered luminescence; ISC, intersystem crossing; ET, energy transfer; IC, internal conversion; S, singlet; T, triplet. Plain arrows indicate radiative transitions; dotted arrows indicate nonradiative transitions. [Reprinted with permission from Cui et al. (2012), Copyright © 2012 American Chemical Society.]

water sensing application. The antenna effect induced by the neutral guest molecule 4,4′-dipyridyl in [Eu_2(adipic acid)$_3$(H_2O)$_2$]·4,4′-dipyridyl (de Lill et al. 2005) was recently reported by de Lill et al. The template (guest) molecule (4,4-dipyridyl) is shown to sensitize the fluorescence of lanthanide metal centers (Eu^{3+}) by guest-host energy transfer after excitation of the guest molecule. More recently, a temperature-controlled guest encapsulation method was reported by Zhang et al. (2010) and the Ln-MOF materials exhibited an efficient light-harvesting property.

Energy transfer from one lanthanide ion to another can also influence the luminescent properties of Ln-MOFs. Guo et al. proposed a method to tune the luminescence by changing the ratio of lanthanide ions (Guo et al. 2010). Due to the energy transfer from Tb^{3+} to Eu^{3+}, the fluorescence intensity at 540 nm changes with the Tb^{3+}/Eu^{3+} ratio. Another example to exploit the energy transfer between Tb^{3+} to Eu^{3+} was illustrated by

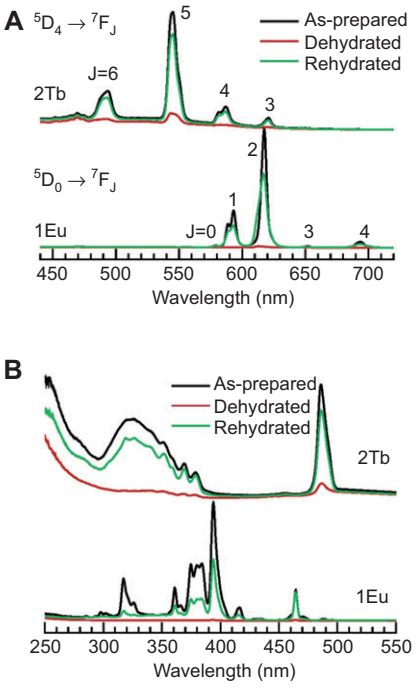

Figure 8 The emission spectra (A) and excitation spectra (B) of 1Eu and 2Tb, their dehydrated and rehydrated phases. For the as-prepared, dehydrated, and rehydrated samples, the measurement was performed under the same instrumental conditions (slits, scanning speed, etc.) at room temperature. The excitation wavelength for emission spectra is 394 nm for Eu and 330 nm for Tb, and the monitor wavelength for excitation spectra is 617 nm for Eu and 545 nm for Tb, respectively. [Reprinted with permission from Zhu et al. (2007), Copyright © 2007 American Chemical Society.]

a Tb(1,3,5-BTC) MOF (Liu et al. 2010). It was observed that among the four bands of the emission spectrum of Tb (1,3,5-BTC)(H_2O)·3H_2O MOF, (correspond to the $^5D_4 \rightarrow {}^7F_5$ transitions of the Tb^{3+}), the strongest band (543 nm) is located in the green region. After doping Tb(1,3,5-BTC) MOF with the Eu^{3+} ion, the luminescence color of the MOF can be easily tuned from green to green-yellow, yellow, orange, and red-orange. That is because of the characteristic emission of the Eu^{3+} in the Eu^{3+} doped MOF, Tb(1,3,5-BTC)(H_2O)·3H_2O:Eu (x=0.1–10 mol %). With the increase in Eu^{3+} concentration, the luminescence intensity of the Tb^{3+} decreases, while that of the Eu^{3+} increases, which caused the color change (Figure 9).

The luminescence of Ln-MOFs can also be tuned by the exchange of metal ions in anionic frameworks. An anionic Ln-MOF $K_5[Tb_5(IDC)_4(ox)_4]$ (IDC=imidazole-4,5-dicarboxylate, ox=oxalate) was presented by Lu et al. (2009) and the cation guest K^+ ions within the frameworks were exchanged with various cations. However, the luminescent intensities of the frameworks exchanged with various cations are quite different (Figure 10A). It was observed that after the addition of Ca^{2+} ions, the emission intensity and the fluorescence lifetime ($^5D_4 \rightarrow {}^7F_5$) of Tb^{3+} was significantly increased (Figure 10B). While some other cations, such as Na^+, NH_4^+, Mg^{2+}, Sr^{2+}, Ba^{2+}, Zn^{2+}, Cd^{2+}, Hg^{2+}, and Pb^{2+} have no influence on the luminescent intensity, transition metal ions of Mn^{2+}, Fe^{2+}, Co^{2+}, Ni^{2+}, and Cu^{2+} can decrease the luminescent intensities.

Recently, there has been an escalating interest in the development of lanthanide near-IR-emitting (NIR) materials because of their potential applications in NIR luminescent optical devices (Guo et al. 2005, White et al. 2009a,b, Yang et al. 2011b). Compared to Eu-MOFs and Tb-MOFs in the visible region, emissive NIR LnMOFs (Ln=Yb, Nd and Er), however, are much less developed, because: (1) it is difficult for most ligands to sensitize Yb^{3+}, Nd^{3+} and Er^{3+}; and (2) the energy gap between the first excited emitting state and the fundamental level of these ions is quite small, thus being easily matched by the C–H, C–C, O–H, and N–H vibrations of the organic ligands. However, it is possible to overcome these limitations by rational design of the MOF structures. This was recently exemplified by White et al. (2009b) in the creation of a luminescent barcoded system based on the multiple NIR emitting of Ln-MOFs (Figure 11). A chromophore ligand, H_2pvdc, was used to excite a series of Ln-MOFs with different amounts of Yb^{3+} and Er^{3+} ions. By controlling the reactant stoichiometry, the relative intensity of the Yb^{3+} and Er^{3+} NIR emissions are linearly correlated to their ratio.

Chemical sensing of microporous Ln-MOFs

The optical properties and luminescence output of Ln-MOFs make them promising candidates for the applications in sensing of cations/anions, small molecules, gases/vapors and some other sensing such as pH, temperature, ionizing radiation and explosives (Xu et al. 2011). Moreover, the porosity within microporous Ln-MOFs can allow the reversible uptake and release of sensing substrates, thus offering the opportunity for the exploration of reversible and recyclable luminescent sensors. The tunable pore size of microporous MOFs may permit the selective recognition and sensing of small molecules, cations and anions. In addition, the open metal sites and functional sites such as Lewis basic/acidic sites within microporous Ln-MOFs can afford different interactions with guest molecules, thus enhancing the sensitivity of the sensors.

One of the widely studied microporous Ln-MOFs is Tb–BTC (MOF-76), which possesses one-dimensional

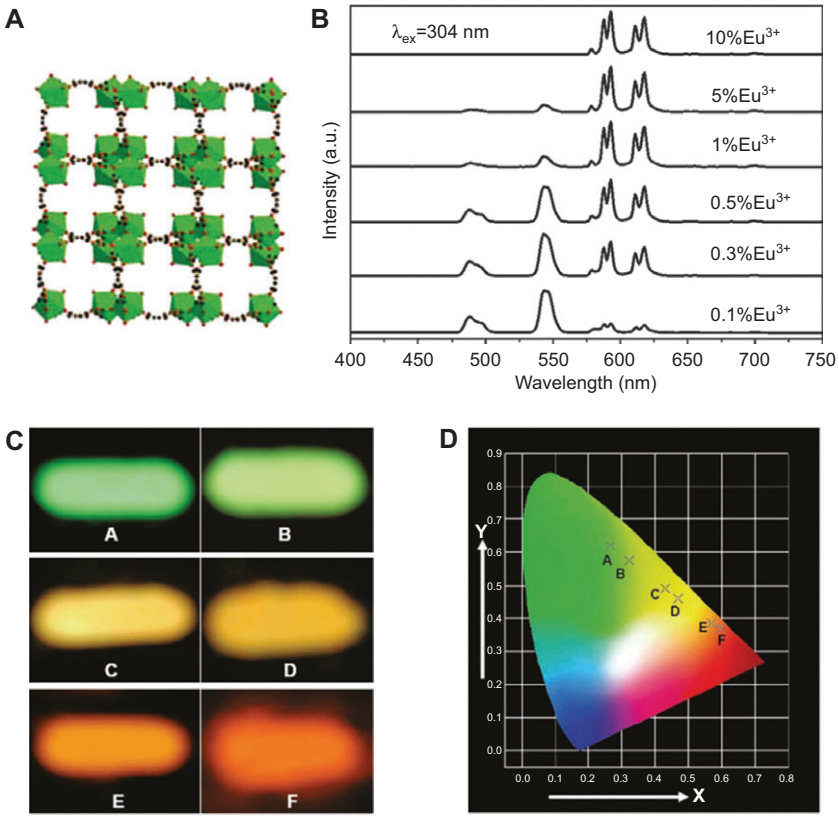

Figure 9 (A) Perspective view of the packing along the c axis of the Tb(1,3,5-BTC)(H_2O)·3H_2O. (B) Emission spectra of the Tb(1,3,5-BTC)-(H_2O)·3H_2O:Eu (x=0.1–10 mol%) under 304 nm excitation. (C) The photographs for the luminescent MOF Tb(1,3,5-BTC)(H_2O)·3H_2O:Eu (x=0 for A, 0.1% for B, 0.3% for C, 0.5% for D, 5% for E, and 10% for F) under excitation of a 254 nm ultraviolet lamp. (D) CIE chromaticity diagram for the Tb(1,3,5-BTC)(H_2O)·3H_2O:Eu. [Reprinted with permission from Liu et al. (2010), Copyright © 2010, The Royal Society of Chemistry.]

channels (6.6×6.6 Å^2), which are partially occupied by the terminal solvent molecules (Figure 12). Chen et al. reported the fluoride sensing property of MOF-76, and discussed the possible mechanisms of the luminescent sensing of MOF-76 (Chen et al. 2008b). The luminescence intensity of MOF-76 increases upon incorporation of different amounts of NaX (X=F^-, Cl^- and Br^-) or Na_2X (X^{2-}=CO_3^{2-} and SO_4^{2-}) in methanol, and the extraordinary enhancement of luminescence intensity was observed for fluoride; this selectivity was also observed in other solvents such as DMF. The authors proposed that the recognition and sensing of anions relied on O-H moieties of the terminal solvents. The hydrogen bonding between the anion and solvent methanol modifies the energy of the O–H bond stretching, leading to the enhancement of luminescence intensity. Moreover, since the hydrogen-bonding interaction between the fluoride anion and the solvent was stronger than other anions, the intensity change was more remarkable than others. Given that the hydrogen bonding interactions with anions can be induced by these N-H and O-H moieties, microporous Ln-MOFs with N–H and O–H containing linkers and terminal organic solvents are promising candidates for anion sensors. The authors also proposed that, owing to the tunable interactions between the terminal solvents and fluoride anions by changing the pore structures and curvatures of Ln-MOFs, more reversible luminescent Ln-MOFs could be realized as anions sensors. Another Ln-BTC, Eu(BTC), which is isostructural with MOF-76, was also reported by Chen et al. for reversible small molecule sensing (Chen et al. 2007).

A different mechanism for recognition and sensing of anions was suggested by Wong et al. for {[Tb(Mucicate)$_{1.5}$(H_2O)$_2$]·5H_2O}$_n$, in which O-H groups of organic linkers are used for the recognition and sensing of anions (Wong et al. 2006). Owing to the large number of OH groups in mucic acid (Figure 13), the hydrogen bonding interaction between the numerous OH groups and anions induced the anion response of the channels. In addition, due to the molecular sieving effect of the microporous frameworks, only small anions are allowed to go through the micropores, while larger anions are blocked.

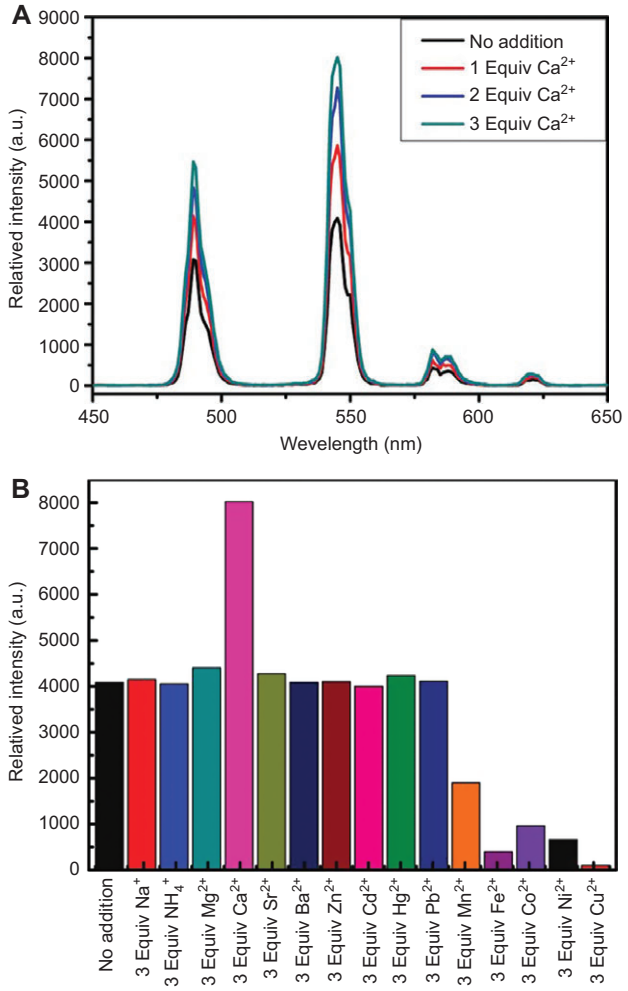

Figure 10 (A) Luminescent intensities of a $^5D_4 \rightarrow {}^7F_5$ transition for an emulsion of $K_5[Tb_5(IDC)_4(ox)_4]$ in DMF (10^{-3} M) at 545 nm upon the addition of various cations (excited at 307 nm). (B) Emission spectra of an emulsion of $K_5[Tb_5(IDC)_4(ox)_4]$ in DMF (10^{-3} M) in the presence of ~0–3 equivalent of Ca^{2+} ions (from $CaCl_2$, excited at 307 nm). [Reprinted with permission from Lu et al. (2009), Copyright © 2009 American Chemical Society.]

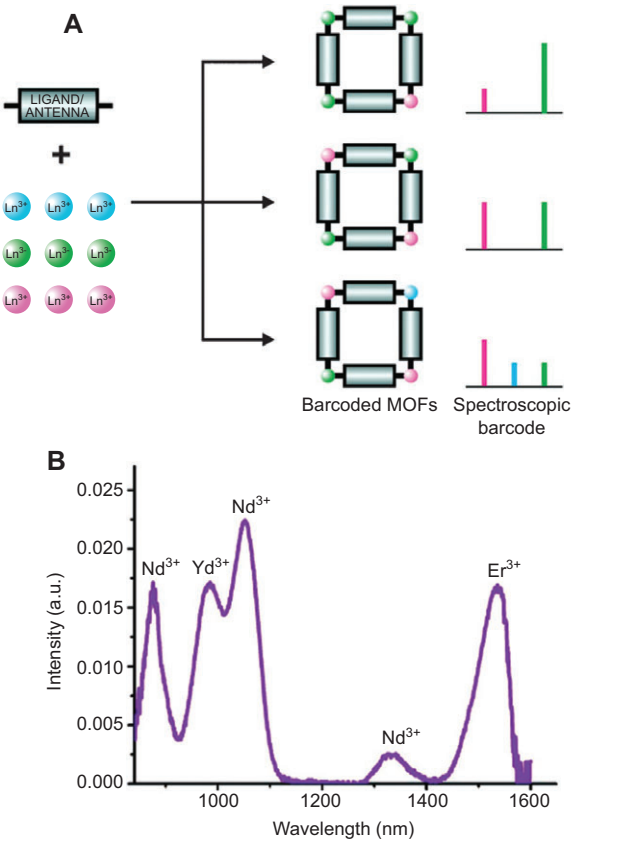

Figure 11 (A) Schematic representation of the approach adopted by White et al. to design photoluminescent barcoded systems based on the use of multiple NIR-emitting Ln^{3+} ions. (B) Nd^{3+}, Yb^{3+} and Er^{3+} emission from $[(Nd_{0.09}Er_{0.55}Yb_{0.36})_2(pvdc)_3(H_2O)_2]\cdot 6DMF\cdot 8.5H_2O$. [Reprinted with permission from White et al. (2009), Copyright © 2009 American Chemical Society.]

The utilization of microporous Ln-MOFs for recognition and sensing of cations has also been explored (Dinca and Long 2008). To make use of the preferential binding of lanthanide ions (Ln^{3+}) to carboxylate oxygen atoms over pyridyl nitrogen atoms, Chen et al. developed a method for synthesizing $[Eu(pdc)_{1.5}(dmf)]\cdot(DMF)_{0.5}(H_2O)_{0.5}$ (pdc=pyridine-3,5-dicarboxylate), which features free Lewis basic pyridyl sites for the recognition and sensing of metal ions (Figure 14) (Chen et al. 2009a). A variety of metal ions (Na^+, K^+, Mg^{2+}, Ca^{2+}, Mn^{2+}, Co^{2+}, Cu^{2+}, Zn^{2+} or Cd^{2+}) were incorporated within $[Eu(pdc)_{1.5}]\cdot DMF$ in DMF solutions, and among them Co^{2+} and Cu^{2+} had the most significant impact on the change of luminescence intensity, owing to their weak binding of the pyridyl nitrogen atoms. It is possible to enhance the selectivity either by constructing porous luminescent MOFs with tuned micropores, or immobilizing various Lewis basic sites to induce preferential binding with respect to different metal ions. In this regard, Chen's group reported a microporous Ln-MOF with highly selectivity in the sensing of Cu^{2+} in aqueous solution (Xiao et al. 2010), and Luo and Batten developed a distinct Ln^{3+}-doped pathway to target MOF-based luminescent sensing of metal ions (Luo and Batten 2010).

Recently, Harbuzaru et al. (2008) reported a very rare example of Ln-MOFs (ITQMOF-1) with a fast response time and rapid reversible behavior for sensing ethanol vapor molecules. ITQMOF-1 possesses a microporous hydrophobic structure based on the ultrahydrophobic ligand 4,4′-(hexafluoroisopropylidene)bis(benzoic acid) (HFIPBB). With the combination of photoluminescent Ln^{3+} centers and the ultrahydrophobic ligand HFIPBB, ITQMOF-1-Eu was used to sense ethanol in air. The air stream was alternatively saturated or unsaturated with ethanol. It was observed that ITQMOF-1-Eu indicated a

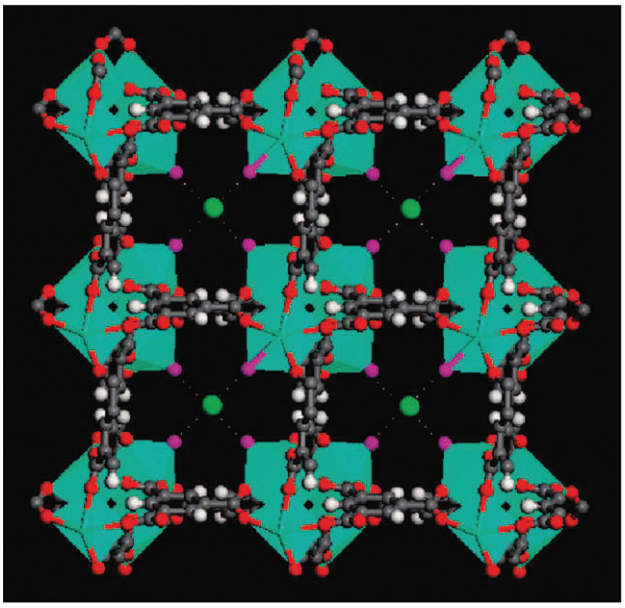

Figure 12 Single crystal X-ray structure of MOF-76b activated in methanol containing NaF with the model of fluoride (green) at the center of the channel involving its hydrogen-bonding interaction with terminal methanol molecules (methanol oxygen, purple; the methyl group from methanol is omitted for clarity). [Reprinted with permission from Chen et al. (2008), Copyright © 2008 American Chemical Society.]

rapid decrease of the emission intensity in the presence of ethanol and a rapid recovery when the sample is exposed to air (Figure 15), and this could be explained by the coordination of ethanol to the Ln^{3+} ions.

The same group also reported an interesting pH sensing material in the pH range of biological interest

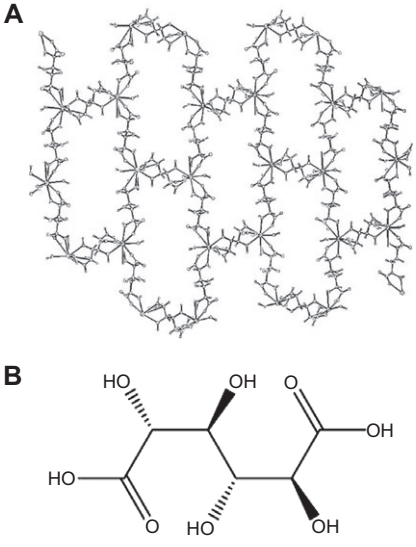

Figure 13 Diagrams of (A) the 2D network of $\{[Tb(Mucicate)_{1.5}(H_2O)_2]\cdot 5H_2O\}_n$, and (B) the structure of mucic acid. [Reprinted with permission from Wong et al. (2006), Copyright © 2006, Wiley-VCH.]

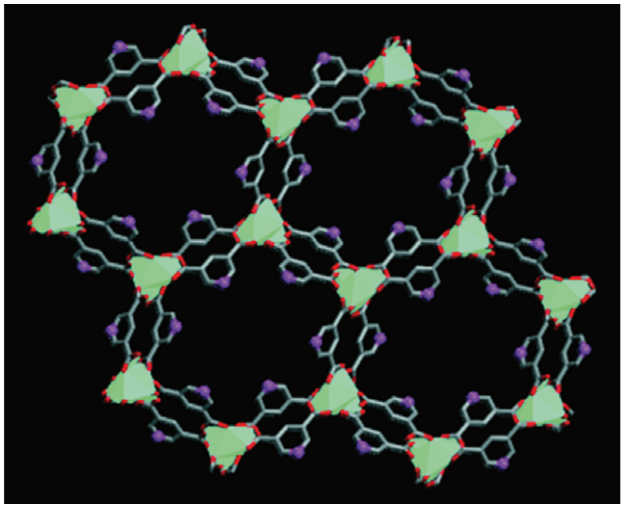

Figure 14 Crystal structure of 1, viewed along crystallographic *a* axis indicating immobilized Lewis basic pyridyl sites oriented towards pore centers. C gray, N purple, O red, Eu green polyhedra. Hydrogen atoms, terminal DMF molecules, and solvent molecules are omitted for clarity. [Reprinted with permission from Chen et al. (2009), Copyright © 2009, Wiley-VCH.]

(5–7.5) (Harbuzaru et al. 2009), based on a photoluminescent Eu-MOF, ITQMOF-3, which contains two different types of Eu^{3+} sites (Eu1 and Eu2). Different from ITQMOF-1, ITQMOF-3 contains a sensitizing ligand H_2PhenDCA (L) and both the carboxylate and phenanthroline moieties of the ligand coordinate to the Eu ion centers (Figure 16). ITQMOF-3 has a layered structure with two different kinds of sheets (sheet A and B), and each kind of sheet contains one type of Eu^{3+} ions (Eu1 or Eu2). These two types of Eu centers display different transition lines in their emission

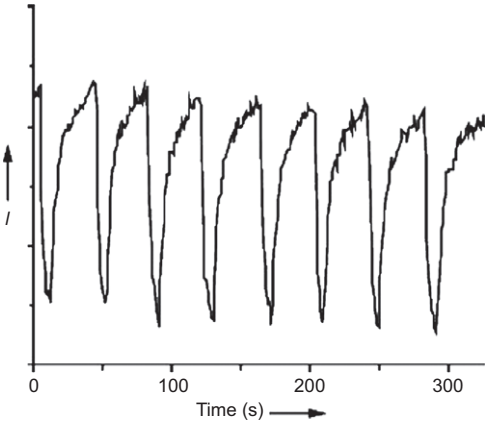

Figure 15 Test for sensing capabilities of the ITQMOF-1-Eu material. Variation of the fluorescence signal intensity at 619 nm under alternating streams of air saturated with ethanol (signal intensity decreases) and ethanol-free air (signal intensity increases). [Reprinted with permission from Harbuzaru et al. (2008), Copyright © 2008, Wiley-VCH.]

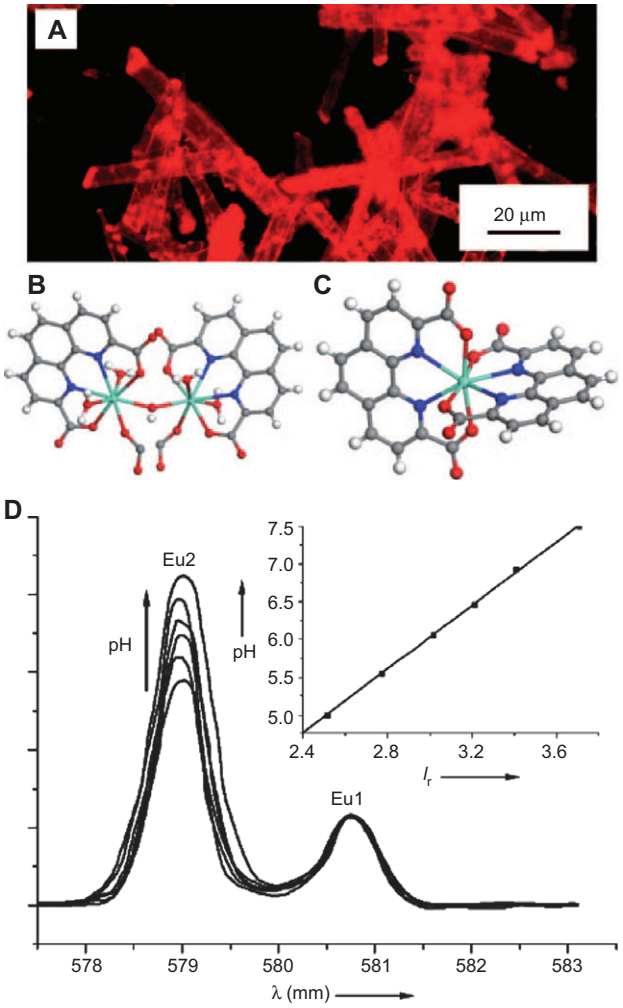

Figure 16 (A) Optical microscopy image of ITQMOF-3-Eu under UV light. (B) Eu2 coordination environment. (C) Eu1 coordination environment. C gray, H white–gray, N blue, Eu green, O red. (D) Intensity variation of the Eu2 $^5D_0$ $^7F_0$ transition from high (pH 7.5) to low (pH 5) pH values; the inset shows the linear variation of Ir with the pH value. [Reprinted with permission from Harbuzaru et al. (2009), Copyright © 2009, Wiley-VCH.]

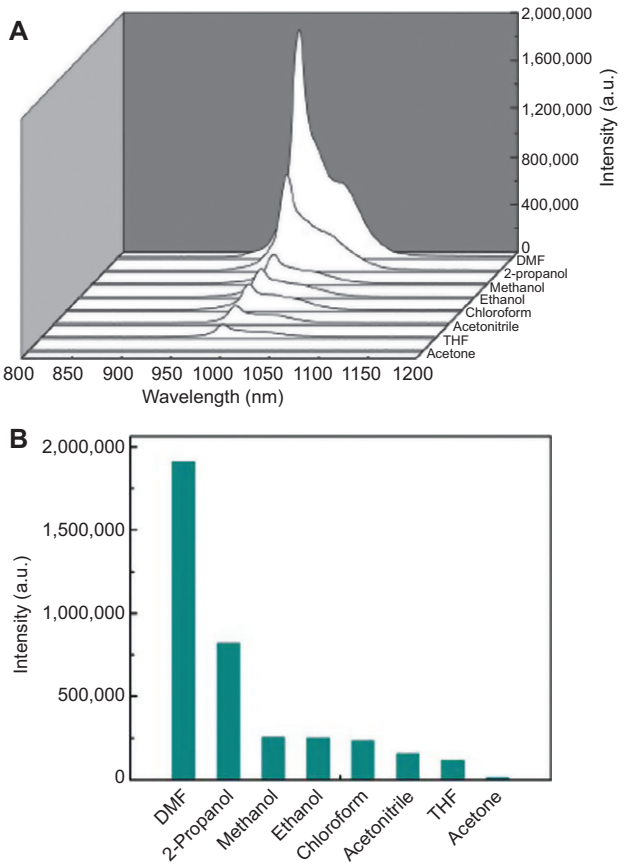

Figure 17 (A) The PL spectra and (B) the $^2F_{5/2}$ $^2F_{7/2}$ transition intensities of 1a introduced into various pure solvent emulsions when excited at 304 nm. [Reprinted with permission from Guo et al. (2011), Copyright © 2011, The Royal Society of Chemistry.]

spectrum. Since the Eu2 center in sheet B forms a dimer with the O-H group, the increase in pH can enhance the intensity of the Eu2 transition line (Figure 16D), which enables ITQMOF-3 to act as a possible miniaturized pH sensor prototype, especially in biological systems.

The sensing of small molecules by microporous Ln-MOFs was recently reported by Guo et al. (2011). A robust and highly porous near infrared (NIR) luminescent Yb-MOF, $Yb(BPT)(H_2O)\cdot(DMF)_{1.5}(H_2O)_{1.25}$ (BPT=biphenyl-3,4′,5-tricarboxylate), was synthesized by the solvothermal reaction of $Yb(NO_3)_3\cdot 6H_2O$ and H_3BPT in mixed solvents of DMF, ethanol, and water, and indicated high selectivity and sensitivity in sensing of various small molecules (Figure 17).

Catalysis application

Unlike homogenous catalysts, heterogeneous catalysts act in a different phase than the reactants, and the major advantage of heterogeneous catalysts lies in the recyclability of catalysts. The most widely used solid-state catalysts in chemical industries are zeolites, which are microporous crystalline materials. Compared to inorganic zeolites, MOFs are usually synthesized under mild conditions, and it is possible to tune their pore/channel sizes and alter the surface functionality by incorporating suitable metal ions or bridging ligands with desired size, shape, chirality, or electronic properties. In addition, the tunable porosity within the frameworks could provide size/shape, or region selectivity, as widely observed in microporous zeolite catalysts. All these have prompted the development of MOFs for heterogeneous catalysis applications (Kesanli and Lin 2003, Kitagawa et al. 2004). The utilization of metal ions as active centers represents one of most common ways to generate catalytically active MOFs (Lee et al. 2009).

Since lanthanide ions have flexible coordination spheres and can create coordinately unsaturated metal centers (Kitagawa et al. 2006), Ln-MOFs have been explored as promising candidates for heterogeneous catalysis.

Of various Ln-MOFs, Tb-MOFs and Eu-MOFs are very attractive because of their versatile coordination geometry and possible high framework stability in water. Choi et al. (2010) reported a Eu-MOF as a photocatalyst for the one-electron oxidation of organic compounds. In this experiment, commercial sources of aromatic sulfides and aliphatic and aromatic amines were used as electron donors after purification. Their findings are encouraging, and demonstrate the possibility that Eu-MOFs could work as efficient photocatalysts under UV light irradiation.

Heterogeneous catalysis performances of a series of 2D lamellar Ln-MOFs were recently reported (Evans et al. 2001, Ngo and Lin 2002), $[Ln(L\text{-}H_2)(L\text{-}H_3)(H_2O)_4]\cdot xH_2O$ (Ln=La, Ce, Pr, Nd, Sm, Gd, Tb, x=9–14,) with the presence of both Lewis and Broństed acid sites. The work showed that the Ln-MOFs could be used as chiral Lewis acid catalysts in the cyanosilylation of aldehydes, ring opening of meso-carboxylic anhydride, and Diels-Alder reactions. Cunha-Silva et al. also reported a series of layered Ln-MOFs with formula as $[Ln(H_2cmp)(H_2O)]$ (Cunha-Silva et al. 2009). The materials were used as solid acid catalysts for the reaction of cyclodehydration of xylose to furfural, and normally give typical 40–77% xylose conversions and 25–42% furfural yields after 4 h reaction, as shown in Table 4. Among these structures, the catalytic performance of $[Y(H_2cmp)(H_2O)]$ was studied in detail. The maximum selectivity was reached at 84% with 83% conversion in the first run, and the solid catalyst could be recycled.

Gustafsson et al. (2010) reported some homeotypic MOFs of $[Ln(btc)(H_2O)]\cdot$guest, all of which have the tetragonal structure containing 1D channels. The materials were assessed as Lewis acid catalysts in the cyanosilylation of aldehydes yielding cyanohydrins. Compared to other MOF catalysts, a higher activity of cyanosilylation of benzaldehyde was observed, and the catalysts were claimed to be recycled and reused without loss of their activity and crystallinity.

Material	Conversion[a] (%)	Selectivity[a] (%)
Y (1)	60	57
La (2)	42	65
Pr (3)	40	62
Nd (4)	77	52
Sm (5)	49	68
Eu (6)	49	67
Gd (7)	45	61
Tb (8)	50	55
Dy (9)	52	79
Ho (10)	43	59
Er (11)	53	53

Table 4 Cyclodehydration of xylose to furfural in the presence of $[RE(H_2cmp)(H_2O)]$ at 443 K. [Reprinted with permission from Cunha-Silva et al. (2009), Copyright © 2009, The Royal Society of Chemistry.]
[a]Calculated for 4 h of reaction.

The solvothermal synthesis of a new family of 3-D isostructural Ln-MOFs with the formula $[Ln_2(pda)_3(H_2O)]\cdot 2H_2O$ was recently reported by Ren et al. (2011). The Ln-MOFs consist of 1D Ln–COO helixes which are cross-linked by the $-CH_2C_6H_4CH_2-$ spacers of the pda^{2-} anions in a 3D compressed honeycomb-shaped network with 1D open channels, which are occupied by guest solvents and coordinated water molecules. Both guest and coordinated water molecules could be removed after activation under dynamic vacuum at 200°C for 4 h, and this afforded the generation of the unsaturated Lewis-acidic metal sites for their catalysis studies. However, of those Ln-MOFs, only $[Tb_2(dpa)_3]$ can efficiently catalyze the acetalization reaction of aldehyde with methanol under mild reaction conditions. Their results showed that a high conversion of 78% could be reached after 10 h reaction, while other Ln-MOFs exhibited low yields even with a longer reaction time. The authors also reported that dehydration and rehydration were reversible for those Ln-MOFs; this demonstrated the possibility of recovery of the catalyst from the heterogeneous reaction mixtures, which was reflected in their experiment data that a 70% high yield of dimethyl acetal was obtained after the third cycle (Table 5).

Several series of rare-earth polymeric frameworks [RPF4 (Gándara et al. 2008), RPF5 (Gándara et al. 2009), RPF9 (Gándara et al. 2010)] were reported, which were prepared on the basis of different kinds of rare-earth coordination polyhedral. These materials can act as active and selective bifunctional heterogeneous catalysts in oxidation reactions of methyl phenyl sulfide. However, the catalytic reactions only took place on the surface of MOFs, because the micropores of the frameworks blocked the substrates from accessing the active metal centers on the pore walls.

Although there have been reported numerous catalytically active Ln-MOFs, the development of microporous Ln-MOFs for heterogeneous catalysis is still at the early stage, and will receive more attention in the near future.

Perspectives

The remarkable structural diversity in combination with the functional organic and inorganic components and porosity,

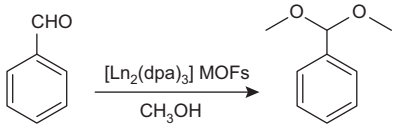

Entry	Catalyst	Time (h)	Conversion (%)[b]
1	–	10	<2
2	$[La_2(dpa)_3]$	10	<5
3	$[Nd_2(dpa)_3]$	10	<5
4	$[Eu_2(dpa)_3]$	10	26
5	$[Yb_2(dpa)_3]$	10	35
6	$[Yb_2(dpa)_3]$	20	56
7	$[Tb_2(dpa)_3]$	10	78
8	$[Tb_2(dpa)_3]$	24	84
9	$[Tb_2(dpa)_3]$	10	75[c], 73[d], 70[e]
10	$[Tb_2(dpa)_3]$	10	22[(f)]
11	$Tb(No_3)_3 \cdot {}^6H_2O$	10	trace

Table 5 Acetalization of benzaldehyde with methanol using a variety of $[Ln_2(dpa)_3]$ MOFs[a] [Reprinted with permission from Ren et al. (2011), Copyright © 2011, Wiley-VCH.]
[a]Reaction conditions: benzaldehyde (1 mmol), catalyst (100 mg), and methanol (3 ml), room temperature. [b]Determined by GC–MS. [c]Yield of first reuse. [d]Yield of second reuse. [e]Yield of third reuse. [f]Reaction was performed in the presence of water (100 µl).

affords microporous Ln-MOFs great potential for various applications, such as gas/solvent adsorption, photoluminescence, chemical sensors, and heterogeneous catalysis as highlighted above. The research of microporous Ln-MOFs is still in its infancy and much remains to be further investigated: (1) because of the highly flexible coordinative behavior of lanthanide metal ions, strategies need to be developed for the construction of extended Ln-MOF structures with large pores and high surface areas; (2) in order to accurately evaluate the luminescence of different samples, it is necessary to incorporate the quantum yield or quantum efficiency in future studies; (3) albeit numerous interesting Ln-MOFs with novel properties have been prepared, the engineering of them into devices for optical, chemical sensor, biomedical detection, and other industrial applications remains a challenge but definitely warrants exploration; (4) the development of porous Ln-MOFs to mimic zeolites for size/shape and region catalysis represents an exciting direction in the field and should be worthy of more attention and dedication. Indeed, with the increasing interest from both academia and industry, microporous Ln-MOFs will remain at the forefront of the materials research, and great progress and breakthroughs in developing them as multifunctional materials will be expected in the near future.

Acknowledgements: The authors acknowledge the University of South Florida for financial support of this work. This work was also supported, in part, by the University of South Florida Internal Awards Program under Grant No.18325.

Received February 28, 2012; accepted June 4, 2012

References

Binnemans, K. Lanthanide-based luminescent hybrid materials. *Chem. Rev*. **2009**, *109*, 4283–4374.

Black, C. A.; Costa, J. S.; Fu, W. T.; Massera, C.; Roubeau, O.; Teat, S. J.; Aromí G.; Gamez, P.; Reedijk, J. 3-D lanthanide metal-organic frameworks: structure, photoluminescence, and magnetism. *Inorg. Chem*. **2009**, *48*, 1062–1068.

Bünzli, J. -C. G. Lanthanide luminescence for biomedical analyses and imaging. *Chem. Rev*. **2010**, *110*, 2729–2755.

Cai, B.; Yang, P.; Dai, W.-J.; Wu, Z.-J. Tuning the porosity of lanthanide MOFs with 2,5-pyrazinedicarboxylate and the first in situ hydrothermal carboxyl transfer. *Cryst. Eng. Comm*. **2011**, *13*, 985–991.

Chandler, B. D.; Yu, J. O.; Cramb, D. T.; Shimizu, G. K. H. Series of lanthanide-alkali metal-organic frameworks exhibiting luminescence and permanent microporosity. *Chem. Mater*. **2007**, *19*, 4467–4473.

Chen, X.-Y.; Zhao, B.; Shi, W.; Xia, J.; Cheng, P.; Liao, D.-Z.; Yan, S.-P.; Jiang, Z.-H. Microporous metal-organic frameworks built on a Ln3 cluster as a six-connecting node. *Chem. Mater*. **2005**, *17*, 2866–2874.

Chen, B.; Yang, Y.; Zapata, F.; Lin, G. N.; Qian, G.; Lobkovsky, E. B. Luminescent open metal sites within a metal-organic framework for sensing small molecules. *Adv. Mater*. **2007**, *19*, 1693–1696.

Chen, L.-F.; Zhang, J.; Ren, G.-Q.; Zhao-Ji, L.; Qin, Y.-Y.; Yin, P.-X.; Cheng, J.-K.; Yao, Y.-G. Nanosized lanthanide oxide rods in I^1O^3 hybrid organic-inorganic frameworks involving *in situ* ligand synthesis. *Cryst. Eng. Comm*. **2008a**, *10*, 1088–1092.

Chen, B.; Wang, L.; Zapata,F.; Qian, G.; Lobkovsky, E. B. A luminescent microporous metal-organic framework for the recognition. *J. Am. Chem. Soc*. **2008b**, *130*, 6718–6719.

Chen, B.; Wang, L. B.; Xiao, Y.; Fronczek, F. R.; Xue, M.; Cui, Y. J.; Qian, G. A luminescent metal-organic framework with Lewis basic pyridyl sites for the sensing of metal ions. *Angew. Chem. Int. Ed*. **2009a**, *48*, 500–503.

Chen, Z.; Zhao, B.; Cheng, P.; Zhao, X.-Q.; Shi, W.; Song, Y. A purely lanthanide-based complex exhibiting ferromagnetic coupling and slow magnetic relaxation behavior. *Inorg. Chem*. **2009b**, *48*, 3493–3495.

Choi, J. R.; Tachikawa, T.; Fujitsuka, M.; Majima, T. Europium-based metal-organic framework as a photocatalyst for the one-electron oxidation of organic compounds. *Langmuir*. **2010**, *26*, 10437–10443.

Connally, R. E.; Piper J. A. Time-gated luminescence microscopy. *J. A. Ann. N. Y. Acad. Sci*. **2008**, *1130*, 106–116.

Cui, Y; Yue, Y.; Qian, G.; Chen, B. Luminescent functional metal-organic frameworks. *Chem. Rev.* **2012**, *112*, 1126–1162.

Cunha-Silva, L.; Lima, S.; Ananias, D.; Silva, P.; Mafra, L.; Carlos, L. D.; Pillinger, M.; Valente, A. A.; Almeida Paz, F. A.; Rocha. J. Multi-functional rare-earth hybrid layered networks: photoluminescence and catalysis studies. *J. Mater. Chem.* **2009**, *19*, 2618–2632.

Datcu, A.; Roques, N.; Jubera, V.; Imaz, I.; Maspoch, D.; Sutter, J.-P.; Rovira, C.; Veciana, J. Three-dimensional porous metal-radical frameworks based on triphenylmethyl radicals. *Chem. Eur. J.* **2011**, *17*, 3644–3656.

de Lill, D. T.; Gunning, N. S.; Cahill, C. L. Toward templated metal-organic frameworks: synthesis, structures, thermal properties, and luminescence of three novel lanthanide-adipate frameworks. *Inorg. Chem*. **2005**, *44*, 258–266.

deKrafft, K. E.; Xie, Z.; Cao, G.; Tran, S., Ma, L.; Zhou, O. Z.; Lin, W. Iodinated nanoscale coordination polymers as potential contrast agents for computed tomography. *Angew. Chem. Int. Ed.* **2009**, *48*, 9901–9904.

Deluzet, A.; Maudez, W.; Daiguebonne, C.; Guillou, O. Interplane distances modulation in lanthanide-based coordination polymers. *Cryst. Growth Des.* **2003**, *3*, 475–479.

Devic, T.; Serre, C.; Audebrand, N.; Marrot, J.; Férey, G. MIL-103, a 3-D lanthanide-based metal organic framework with large one-dimensional tunnels and a high surface area. *J. Am. Chem. Soc*. **2005**, *127*, 12788–12789.

Dinca, M.; Long, J. R. Hydrogen storage in microporous metal-organic frameworks with exposed metal sites. *Angew. Chem. Int. Ed.* **2008**, *47*, 6766–6779.

Eliseeva, S. V.; Bünzli, J. -C. G. Lanthanide luminescence for functional materials and bio-sciences. *Chem. Soc. Rev*. **2010**, *39*, 189–227.

Evans, O. R.; Ngo, H. L.; Lin, W. B. Chiral porous solids based on lamellar lanthanide phosphonates. *J. Am. Chem. Soc.* **2001**, *123*, 10395–10396.

Farha, O.; Malliakas, C. D.; Kanatzidis, M. G.; Hupp, J. T. Control over catenation in metal-organic frameworks via rational design of the organic building block. *J. Am. Chem. Soc*. **2010**, *132*, 950.

Férey, G. Hybrid porous solids: past, present, future. *Chem. Soc. Rev*. **2008**, *37*, 191–214.

Gándara, F.; García-Cortés, A.; Cascales, C.; Gómez-Lor, B.; Gutiérrez-Puebla, E.; Iglesias, M.; Monge, A.; Snejko, N. Rare earth arenedisulfonate metal-organic frameworks: an approach toward polyhedral diversity and variety of functional compounds. *Inorg. Chem.* **2007**, *46*, 3475–3484.

Gándara, F.; Andrés, A. D.; Gómez-Lor, B.; Gutiérrez-Puebla, E.; Iglesias, M.; Monge, M. A.; Proserpio, D. M.; Snejko, N. A rare-earth MOF Series: fascinating structure, efficient light emitters, and promising catalysts. *Cryst. Growth Des*. **2008**, *8*, 378–380.

Gándara, F.; Gutiérrez-Puebla, E.; Iglesias, M.; Proserpio, D. M.; Snejko, N.; Monge, M. A. Controlling the structure of arenedisulfonates toward catalytically active materials. *Chem. Mater*. **2009**, *21*, 655–661.

Gándara, F.; Gutiérrez-Puebla, E.; Iglesias, M.; Snejko, N.; Monge, M. A. Isolated hexanuclear hydroxo lanthanide secondary building units in a rare-earth polymeric framework based on p-sulfonatocalix[4]arene. *Cryst. Growth Des*. **2010**, *10*, 128–134.

Ghosh, S. K.; Bharadwaj, P. K. Self-assembly of lanthanide helicate coordination polymers into 3D metal-organic framework structures. *Inorg. Chem.* **2004**, *43*, 2293–2298.

Gu, Z.-G.; Fang, H.-C.; Yin, P.-Y.; Tong, L.; Ying, L.; Hu, S.-J.; Li, W.-S.; Cai, Y.-P. A family of three-dimensional lanthanide-zinc heterometal-organic frameworks from 4,5-imidazoledicarboxylate and oxalate. *Cryst. Growth Des*. **2011**, *11*, 2220–2227.

Guo, X.; Zhu, G.; Fang, Q.; Xue, M.; Tian, G.; Sun, J.; Li, X.; Qiu, S. Synthesis, structure and luminescent properties of rare earth coordination polymers constructed from paddle-wheel building blocks. *Inorg. Chem*. **2005**, *44*, 3850–3855.

Guo, X.; Zhu, G.; Li, Z.; Sun, F.; Yang, Z.; Qiu, S. A lanthanide metal-organic framework with high thermal stability and available Lewis-acid metal sites. *Chem. Commun*. **2006a**, *42*, 3172–3174.

Guo, X.; Zhu, G.; Sun, F.; Li, Z.; Zhao, X.; Li, X.; Wang, H.; Qiu, S. Synthesis, structure, and luminescent properties of microporous lanthanide metal-organic frameworks with inorganic rod-shaped building units. *Inorg. Chem*. **2006b**, *45*, 2581–2587.

Guo, H.; Zhu, Y.; Qiu, S.; Lercher, J. A.; Zhang, H. Coordination modulation induced synthesis of nanoscale Eu_{1-x} Tb_x-metal-organic frameworks for luminescent thin films. *Adv. Mater*. **2010**, *22*, 4190–4192.

Guo, Z; Xu, H.; Su, S.; Cai, J.; Dang, S.; Xiang, S. A robust near infrared luminescent ytterbium metal-organic framework for sensing of small molecules. *Chem. Commun*. **2011**, *47*, 5551–5553.

Gustafsson, M.; Bartoszewicz, A.; Martin-Matute, B; Sun, J. L.; Grins, J.; Zhao, T.; Li, Z. Y.; Zhu, G. S.; Zou, X. D. A family of highly stable lanthanide metal-organic frameworks: structural evolution and catalytic activity. *Chem. Mater.* **2010**, *22*, 3316–3322.

Han, Y.; Li, X.; Li, L.; Ma, C.; Shen, Z.; Song, Y.; You, X. Structures and properties of porous coordination polymers based on lanthanide carboxylate building units. *Inorg. Chem.* **2010**, *49*, 10781–10787.

Harbuzaru, B. V.; Corma, A.; Rey, F.; Atienzar, P.; Jordá, J. L.; García, H.; Ananias, D.; Carlos, L. D.; Rocha, J. Metal-organic nanoporous structures with anisotropic photoluminescence and magnetic properties and their use as sensors. *Angew. Chem. Int. Ed.* **2008**, *47*, 1080–1083.

Harbuzaru, B. V.; Corma, A.; Rey, F.; Jorda, J. L.; Ananias, D.; Carlo, L. D.; Rocha, J. A miniaturized linear pH sensor based on a highly photoluminescent self-assembled Europium(III) metal-organic framework. *Angew. Chem., Int. Ed.* **2009**, *48*, 6476–6479.

He, H.; Yuan, D.; Ma, H.; Sun, D.; Zhang, G.; Zhou, H.-C. Control over interpenetration in lanthanide-organic frameworks: synthetic strategy and gas-adsorption properties. *Inorg. Chem*. **2010**, *49*, 7605–7607.

Huang, W.; Wu, D.; Zhou, P.; Yan, W. B.; Guo, D.; Duan, C. Y.; Meng, Q. J. Luminescent and magnetic properties of lanthanide-thiophene-2,5-dicarboxylate hybrid materials. *Cryst. Growth Des*. **2009**, *9*, 1361–1369.

Jiang, H.-L.; Tsumori, N.; Xu, Q. A Series of (6,6)-connected porous lanthanide-organic framework enantiomers with high thermostability and exposed metal sites: scalable syntheses, structures, and sorption properties. *Inorg. Chem*. **2010a**, *49*, 10001–10006.

Jiang, J.-J.; Pan, M.; Liu J.-M.; Wang, W.; Su, C. Y. Assembly of robust and porous hydrogen-bonded coordination frameworks: isomorphism, polymorphism, and selective adsorption. *Inorg. Chem*. **2010b**, *49*, 10166–10173.

Kesanli, B.; Lin, W. B. Chiral porous coordination networks: rational design and applications in enantioselective processes. *Coord. Chem. Rev*. **2003**, *246*, 305–326.

Khan, N. A.; Haque, M. M.; Jhung, S. H. Accelerated syntheses of porous isostructural lanthanide–benzenetricarboxylates (Ln–BTC) under ultrasound at room temperature. *Eur. J. Inorg. Chem.* **2010**, *31*, 4975–4981.

Kitagawa, S.; Kitaura, R.; Noro, S. I. Functional porous coordination polymers. *Angew. Chem. Int. Ed*. **2004**, *43*, 2334–2375.

Kitagawa, S.; Noro, S.-I.; Nakamura, T. Pore surface engineering of microporous coordination polymers. *Chem. Commun*. **2006**, *7*, 701–707.

Knope, K. E.; de Lill, D. T.; Rowland, C. E.; Catons, P. M.; Betencourt-Dias, A.; Cahill, C. L. Uranyl sensitization of samarium(III) luminescence in a two-dimensional coordination polymer. *Inorg. Chem*. **2012**, *51*, 201–206.

Kondo, M.; Shimamura, M.; Noro, S.; Minakoshi, S.; Asami, A.; Seki, K.; Kitagawa, S. Microporous materials constructed from the interpenetrated coordination networks: structures and methane adsorption properties. *Chem. Mater.* **2000**, *12*, 1288–1299.

Kostakis, G. E.; Abbas, G.; Anson, C. E.; Powell, A. K. Inclusion of a well resolved T4(2)6(2) water tape in a H-bonded, (4,7)-binodal 3D network. *Cryst. Eng. Comm.* **2009**, *11*, 82–86.

Lan, M. H.; Pan, M.; Eichhcfer, A.; Fenske, D.; Su, C. Y. Thermally stable porous hydrogen-bonded coordination networks displaying dual properties of robustness and dynamics upon guest uptake. *Chem. Eur. J.* **2010**, *16*, 1841–1848.

Lee, J. Y.; Farha, O. K.; Roberts, J.; Scheidt, K. A.; Nguyen, S. T.; Hupp, J. T. Metal-organic framework materials as catalysts. *Chem. Soc. Rev*. **2009**, *38*, 1450–1459.

Lee, W. R.; Ryu, D. W.; Lee, J. W.; Yoon, J. H.; Koh, E. K.; Hong, C. S. Microporous lanthanide-organic frameworks with open metal sites: unexpected sorption propensity and multifunctional properties. *Inorg. Chem.* **2010**, *49*, 4723–4725.

Liang, G.; Xu, J.; Wang, X. Synthesis and characterization of organo-metallic coordination polymer nanoshells of Prussian blue using miniemulsion periphery polymerization (MEPP). *J. Am. Chem. Soc.* **2009**, *131*, 5378–5379.

Liao, W.; Liu, C.; Wang, X.; Zhu, G.; Zhao, X.; Zhang, H. 3D metal-organic frameworks incorporating water-soluble tetra-p-sulfonatocalix[4]arene. *Cryst. Eng. Comm.* **2009**, *11*, 2282–2284.

Lim, Y. T.; Noh, Y.-W.; Cho, J.-H.; Han, J. H.; Choi, B. S.; Kwon, J.; Hong, K. S.; Gokarna, A.; Cho Y.-H.; Chung, B. H. Multiplexed imaging of therapeutic cells with multispectrally encoded magnetofluorescent nanocomposite emulsions. *J. Am. Chem. Soc.* **2009**, *131*, 17145–17154.

Lin, Y.-W.; Jian, B.-R.; Huang, S.-C.; Huang, C.-H.; Hsu, K.-F. Synthesis and characterization of three ytterbium coordination polymers featuring various cationic species and a luminescence study of a terbium analogue with open channels. *Inorg. Chem*. **2010**, *49*, 2316–2324.

Liu, K.; You, H.; Zheng, Y.; Jia, G.; Song, Y.; Huang, Y.; Yang, M.; Jia, J.; Guo, N.; Zhang, H. Facile and rapid fabrication of metal-organic framework nanobelts and color-tunable photoluminescence properties. *J. Mater. Chem*. **2010**, *20*, 3272–3279.

Liu, T.-F.; Zhang, W.; Sun, W.-H., Cao, R. Conjugated ligands modulated sandwich structures and luminescence properties of lanthanide metal-organic frameworks. *Inorg. Chem*. **2011**, *50*, 5242–5248.

Lu, W.-G.; Jiang, L.; Feng, X.-L.; Lu, T.-B. Three-dimensional lanthanide anionic metal-organic frameworks with tunable luminescent properties induced by cation exchange. *Inorg. Chem*. **2009**, *48*, 6997–6999.

Luo, J.; Xu, H.; Liu, Y.; Zhao, Y.; Daemen, L. L.; Brown, C.; Timofeeva, T. V.; Ma, S.; Zhou, H.-C. Hydrogen adsorption in a highly stable porous rare-earth metal-organic framework: sorption properties and neutron diffraction studies. *J. Am. Chem. Soc*. **2008**, *130*, 9626–9627.

Luo, F.; Batten, S. R. Metal-organic framework (MOF): lanthanide(III)-doped approach for luminescence modulation and luminescent sensing. *Dalton Trans*. **2010**, *39*, 4485–4488.

Ma, S.; Sun, D.; Ambrogio, M.; Fillinger, J. A.; Parkin, S.; Zhou, H.-C. Framework-catenation isomerism in metal-organic frameworks and its impact on hydrogen uptake. *J. Am. Chem. Soc.* **2007**, *129*, 1858–1859.

Ma, L. Q.; Lin, W. B. Chirality-controlled and solvent-templated catenation isomerism in metal-organic frameworks. *J. Am. Chem. Soc.* **2008a**, *130*, 13834–13835.

Ma, S.; Wang, X.-S.; Yuan, D.; Zhou, H.-C. A coordinatively linked Yb metal-organic framework demonstrates high thermal stability and uncommon gas-adsorption selectivity. *Angew. Chem., Int. Ed.* **2008b**, *47*, 4130.

Ma, S.; Yuan, D.; Wang, X.-S.; Zhou, H.-C. Microporous lanthanide metal-organic frameworks containing coordinatively linked interpenetration: syntheses, gas adsorption studies, thermal stability analysis, and photoluminescence investigation. *Inorg. Chem*. **2009**, *48*, 2072–2077.

Ma, S.; Zhou, H.-C. Gas storage in porous metal-organic frameworks for clean energy applications. *Chem. Commun*. **2010**, *46*, 44–53.

McHale, R.; Ghasdian, N.; Liu, Y.; Wang, H.; Miao, Y; Wang, X. Synthesis of prussian blue coordination polymer nanocubes via confinement of the polymerization field using miniemulsion periphery polymerization (MEPP). *Macromol. Rapid Commun*. **2010**, *31*, 856–860.

Mohapatra, S.; Hembram, K.; Waghmare, U.; Maji, T. Immobilization of alkali metal ions in a 3d lanthanide-organic framework: selective sorption and H2 storage characteristics. *Chem. Mater*. **2009**, *21*, 5406–5412.

Moore, E. G.; Samuel, A. P. S.; Raymond, K. N. From antenna to assay: lessons learned in lanthanide luminescence. *Acc. Chem. Res.* **2009**, *42*, 542–552.

Nayak, S.; Nayek, H. P.; Pietzonka, C.; Novitchi, G.; Dehnen, S. A series of three-dimensional lanthanide MOFs: observation of reversible structural changes controlled by solvent desorption–adsorption, and magnetic properties. *J. Mol. Struct.* **2011**, *1004*, 82–87.

Ngo, H. L.; Lin, W. Chiral crown ether pillared lamellar lanthanide phosphonates. *J. Am. Chem. Soc.* **2002**, *124*, 14298–14299.

Ni, Z.; Masel, R. I. Rapid production of metal-organic frameworks via microwave-assisted solvothermal synthesis. *J. Am. Chem. Soc.* **2006**, *128*, 12394–12395.

Pereira, G. A.; Peters, J. A.; Paz, F. A. A.; Rocha, J.; Geraldes, C. F. G. C. Evaluation of [Ln(H_2cmp)(H_2O)] metal organic framework materials for potential application as magnetic resonance imaging contrast agents. *Inorg. Chem.* **2010**, *49*, 2969–2974.

Reineke, T. M.; Eddaoudi, M.; Fehr, M.; Kelley, D.; Yaghi, O. M. From condensed lanthanide coordination solids to microporous frameworks having accessible metal sites. *J. Am. Chem. Soc.* **1999**, *121*, 1651–1657.

Ren, Y. W.; Liang, J. X.; Lu, J. X.; Cai, B. W.; Shi, D. B.; Qi, C. R.; Jiang, H. F.; Chen, J.; Zheng, D. 1,4-Phenylenediacetate-based Ln MOFs–synthesis, structures, luminescence, and catalytic activity. *Eur. J. Inorg. Chem.* **2011**, *28*, 4369–4376.

Rieter, W. J.; Taylor, K. M. L.; Lin, W. Surface modification and functionalization of nanoscale metal-organic frameworks for controlled release and luminescence sensing. *J. Am. Chem. Soc.* **2007**, *129*, 9852–9853.

Rocha, J.; Paz, F. A. A.; Shi, F. N.; Ferreira, R. A. S.; Trindade, T.; Carlos, L. D. Photoluminescent porous modular lanthanide-vanadium-organic frameworks. *Eur. J. Inorg. Chem.* **2009**, *33*, 4931–4945.

Rocha, J.; Carlos, L. D.; Almeida Paz, F. A.; Ananias, D. Multifunctional luminescent lanthanides-based metal-organic frameworks. *Chem. Soc. Rev*. **2011**, *40*, 926–940.

Roques, N.; Maspoch, D.; Imaz, I.; Datcu, A.; Sutter, J.-P.; Rovira, C.; Veciana, J. A three dimensional lanthanide-organic radical open-framework. *Chem. Comm*. **2008**, *27*, 3160–3162.

Rosi, N. L.; Kim, J.; Eddaoudi, M.; Chen, B. L.; O'Keeffe, M.; Yaghi, O. M. Rod packings and metal-organic frameworks constructed from rod-shaped secondary building units. *J. Am. Chem. Soc*. **2005**, *127*, 1504–1518.

Shekhah, O.; Wang, H.; Paradinas, M.; Ocal, C.; Schupbach, B.; Terfort, A.; Zacher, D.; Fischer, R. A.; Woll, C. Controlling interpenetration in metal-organic frameworks by liquid phase epitaxy. *Nat. Mater.* **2009**, *8*, 481–484.

Silva, P.; Valente, A. A.; Rocha, J.; Paz, F. A. A. Fast microwave synthesis of a microporous lanthanide-organic framework. *Cryst. Growth Des*. **2010**, *10*, 2025–2028.

Snejko, N.; Cascales, C.; Gomez-Lor, B.; Gutierrez- Puebla, E.; Iglesias, M.; Ruiz-Valero, C.; Monge, A. From rational octahedron design to reticulation serendipity. A thermally stable rare earth polymeric disulfonate family with CdI_2-like structure, bifunctional catalysis and optical properties. *Chem. Commun*. **2002**, *13*, 1366–1367.

Sun, Y.-G.; Jiang, B.; Cui, T.-F.; Xiong, G.; Smet, P. F.; Ding, F.; Gao, E.-J.; Lv, T.-Y., Eeckhout, K. V.; Poelman, D.; Verpoort, F. Solvothermal synthesis, crystal structure, and properties of lanthanide-organic frameworks based on thiophene-2,5-dicarboxylic acid. *Dalton Tran.* **2011**, *40*, 11581–11590.

Tanaka, D.; Henke, A.; Albrecht, K.; Moeller, M.; Nakagawa, K.; Kitagawa, S.; Groll, J. Rapid preparation of flexible porous coordination polymer nanocrystals with accelerated guest adsorption kinetics. *Nat. Chem*. **2010**, *2*, 410–416.

Taylor, K. M. L.; Jin, A.; Lin, W. Surfactant-assisted synthesis of nanoscale gadolinium metal-organic frameworks for potential multimodal imaging. *Angew. Chem. Int. Ed*. **2008**, *47*, 7722–7725.

Taylor, K. M. L.; Rieter, W. J.; Lin, W. Manganese-b ased nanoscale metal-organic frameworks for magnetic resonance imaging. *J. Am. Chem. Soc.* **2008**, *130*, 14358–14359.

Wang, Z.; Jin, C. M.; Shao, T.; Li, Y. Z.; Zhang, K. L.; Zhang, H. T.; You, X. Z. Syntheses, structures, and luminescence properties of a new family of three-dimensional open-framework lanthanide coordination polymers. *Inorg. Chem. Commun.* **2002**, *5*, 642–648.

Wang, X.-W.; Zheng, S.-T.; Liu, W.; Yang, G.-Y. An unusual eight-connected self-penetrating ilc net constructed by dinuclear lanthanide building units. *Cryst. Eng. Comm.* **2008**, *10*, 765–769.

Wang, M.-X., Long, L.-S.; Huang, R.-B.; Zheng, L.-S. Influence of halide ions on the chirality and luminescent property of ionothermally synthesized lanthanide-based metal–organic frameworks. *Chem. Comm*. **2011**, *47*, 9834–9836.

White, K. A.; Chengelis, D. A.; Zeller, M.; Geib, S. J.; Szakos, J.; Petoud S.; Rosi, N. L. Near-infrared emitting ytterbium metal-organic frameworks with tunable excitation properties. *Chem. Commun.* **2009a**, *30*, 4506–4508.

White, K. A.; Chengelis, D. A.; Gogick, K. A.; Stehman, J.; Rosi N. L.; Petoud, S. Near-infrared luminescent lanthanide MOF barcodes. *J. Am. Chem. Soc*. **2009b**, *131*, 18069–18071.

Wong, K.-L.; Law, G.-L.; Yang, Y.-Y.; Wong, W.-T. A highly porous luminescent terbium-organic framework for reversible anion sensing. *Adv. Mater*. **2006**, *18*, 1051–1054.

Xiao, Y.; Cui, Y.; Zheng, Q.; Xiang, S.; Qian, G.; Chen, B. A microporous luminescent metal-organic framework for highly selective and sensitive sensing of Cu^{2+} in aqueous solution. *Chem. Commun.* **2010**, *46*, 5503–5505.

Xu, H.; Liu, F.; Cui, Y.; Chen, B.; Qian, G. A luminescent nanoscale metal-organic framework for sensing of nitroaromatic explosives. *Chem. Commun*. **2011**, *47*, 3153–3155.

Yang, J.; Song, S. Y.; Ma, J. F.; Liu, Y. Y.; Yu, Z. T. Syntheses, structures, photoluminescence, and gas adsorption of rare earth-organic frameworks based on a flexible tricarboxylate. *Cryst. Growth Des*. **2011a**, *11*, 5469–5474.

Yang, Q.-Y.; Li, K.; Luo, J.; Pan, M.; Su, C.-Y. A simple topological identification method for highly (3,12)-connected 3D MOFs showing anion exchange and luminescent properties. *Chem. Comm.* **2011b**, *47*, 4234–4236.

Zhang, J. J.; Wojtas, L.; Larsen, R. W.; Eddaoudi, M.; Zaworotko, M. J. Temperature and concentration control over interpenetration in a metal-organic material. *J. Am. Chem. Soc*. **2009**, *131*, 17040–17041.

Zhang, X.; Ballem, M. A.; Ahrén, M.; Suska, A.; Bergman, P.; Uvdal, K. Nanoscale Ln(III)-carboxylate coordination polymers (Ln=Gd, Eu, Yb): temperature-controlled guest encapsulation and light harvesting. *J. Am. Chem. Soc*. **2010**, *132*, 10391–10397.

Zhang, X.; Ballem, M. A.; Hu, Z.-J.; Bergman, P.; Uvdal, K. Nanoscale light-harvesting metal–organic frameworks. *Angew. Chem. Int. Ed*. **2011**, *50*, 5729–5733.

Zhao, B.; Cheng, P.; Chen, X.; Cheng, C.; Shi, W.; Liao, D.; Yan, S.; Jiang, Z. Design and synthesis of 3d-4f metal-based zeolite-type materials with a 3D nanotubular structure encapsulated "water" pipe. *J. Am. Chem. Soc.* **2004**, *126*, 3012–3013.

Zhao, X.-Q.; Zuo, Y.; Gao, D.-L.; Zhao, B.; Shi, W.; Cheng, P. Syntheses, structures, and luminescence properties of a series of Ln III – Ba II heterometal-organic frameworks. *Cryst. Eng. Comm*. **2009a**, *9*, 3948–3957.

Zhao, X.-Q.; Zhao, B.; Shi, W.; Cheng, P. Structures and luminescent properties of a series of Ln–Ag heterometallic coordination polymers. *Cryst. Eng. Comm.* **2009b**, *11*, 1261–1269.

Zhao, X.; Zhu, G.; Fang, Q.; Wang, Y.; Sun, F.; Qiu, S. A series of three-dimensional lanthanide coordination compounds with the rutile topology. *Cryst. Growth Des*. **2009c**, *9*, 737–742.

Zhao, X.-J.; Ben, T.; Xue, M.; Zhu, G.-S.; Fang, Q.-R.; Qiu, S.-L. A rare 3D lanthanide metal-organic framework with the rutile topology: synthesis, structure and properties. *J. Mol. Struct.* **2009d**, *931*, 25–30.

Zhu, W., Wang, Z.; Gao, S. Two 3D porous lanthanide-fumarate-oxalate frameworks exhibiting framework dynamics and luminescent change upon reversible de- and rehydration. *Inorg. Chem.* **2007**, *46*, 1337–1342.

Yao Chen
Department of Chemistry
University of South Florida
4202 E. Fowler Avenue
Tampa, FL 33620
USA

Yao Chen obtained her BS degree from Qingdao University of Science & Technology in 2006, and received her MS degree from Nanjing University of Technology in 2009 under the supervision of Dr. He Huang. She is currently a PhD student in the Department of Chemistry at University of South Florida, under the supervision of Dr. Shengqian Ma. Her research interest focuses on the development of functional porous MOF materials for biological-related applications.

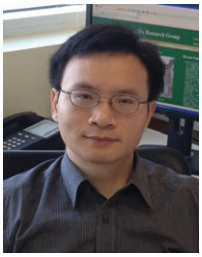

Shengqian Ma
Department of Chemistry
University of South Florida
4202 E. Fowler Avenue
Tampa, FL 33620
USA
sqma@usf.edu

Dr. Shengqian Ma received his B.S. degree from Jilin University, China in 2003, and graduated from Miami University (Ohio) with a PhD degree under the supervision of Hong-Cai Joe Zhou (currently at Texas A&M University) in 2008. After finishing a 2-year Director's Postdoctoral Fellowship at Argonne National Laboratory, he joined the Department of Chemistry at University of South Florida as an Assistant Professor in August 2010. His research interest focuses on the development of functional porous materials for energy and biological-related applications.